TECHNISCHE UNIVERSITÄT WIEN

DIPLOMARBEIT

Optimizing a DNA Origami-Based Model System to Assess T-Cell Activation

zur Erlangung des akademischen Grades
Diplom-Ingenieurin

im Rahmen des Studiums
Biomedical Engineering

ausgeführt am Institut für Angewandte Physik der Fakultät Physik in der Forschungsgruppe für Biophysik
der Technischen Universität Wien

unter der Anleitung von

Associated Prof. Dipl.-Ing.in Dr.in techn. Eva Sevcsik

und

Anežka Májková, MSc

durch

Daniela Schalmer, BSc
Matrikelnummer: 01607439

Unterschrift Betreuer

Wien, 12.03.2025

Unterschrift Verfasserin

Zusammenfassung

Die Rolle von geclusterten T-Zell-Rezeptoren in der Aktivierung von T-Zellen und inwiefern vorgeclusterte Liganden diesen Prozess fördern können, sind weiterhin Gegenstand wissenschaftlicher Diskussionen. Eine Möglichkeit zur Klärung dieser Fragestellung, bietet der Einsatz von Modell-Systemen, da sie die Erforschung von biologischen Prozessen auf molekularem Level ermöglichen. In der vorliegenden Arbeit wurde ein bestehendes Protokoll zur Erstellung eines Modell-Systems basierend auf DNA-Origamis und Lipid-Doppelschichten auf festem Substrat (SLBs) untersucht und optimiert. Ziel der Arbeit war die Entwicklung eines zuverlässigen Systems zur Untersuchung der T-Zell-Aktivierung. Zu diesem Zweck wurden vier essentielle Schritte des Protokolls analysiert: der thermale Faltungsprozess von DNA-Origamis, die Aufreinigung von gefalteten Plattformen, die Funktionalisierung von DNA-Origami-Plattformen und die Verankerung der Plattformen auf den SLBs. Ein optimiertes Faltungsprotokoll wurde entwickelt, bei dem der Fokus auf sowohl Zuverlässigkeit als auch Zeit-Effizienz gelegt wurde. Aufgrund des reduzierten Arbeitsaufwandes wurde die Ultra-Filtration als bevorzugte Aufreinigungsmethode gewählt. Bei der Plattformverankerung konnte die $MgCl_2$-unterstützte Methode mit verbesserten Oberflächendichten überzeugen. Zudem zeigte sich, dass die Plattformfunktionalisierung signifikant bessere Ergebnisse erzielt, wenn sie am Tag des Experiments durchgeführt wird. Zusammenfassend liefert diese Arbeit wertvolle Einblicke in die essenziellen Schritte der Erstellung eines DNA-Origami-basierten Modell-Systems und trägt dazu bei, ein zuverlässiges System zur Untersuchung der T-Zell-Aktivierung zu etablieren. Die gewonnenen Erkenntnisse bieten Forschern eine fundierte Grundlage zur Entwicklung eigener Protokolle für weiterführende Studien.

Abstract

The role of microclustering of T-cell receptors (TCRs) in T-cell activation, and whether pre-clustered ligands can promote this clustering and thus facilitate activation, remains a subject of ongoing investigation. A convenient approach to investigate this question is to use model systems, as they allow researchers to dissect biological processes at the molecular level. In this thesis, an existing protocol for the creation of such a model system based on DNA origami and supported lipid bilayers (SLBs) was optimized with the aim of producing a reliable system that could be used for the assessment of T-cell activation. To this end, the thermal folding process of DNA origami, the purification of folded platforms, the functionalization of DNA origami platforms, and the anchoring of platforms to SLBs were analyzed and refined. An optimized thermal folding protocol was developed, with a focus on reliability as well as time efficiency. Ultra-filtration was identified as a more efficient purification method than agarose gel electrophoresis due to its reduced labor intensity and time requirements. Platform anchoring was found to be more stable when mediating cholesterol anchoring with $MgCl_2$, and platform binding efficiency of pMHC was found to be clearly higher when functionalizing platforms on the day of the experiment. In conclusion, the work provided insight into the essential steps in the creation of a DNA origami-based model system, helping to create a reliable model system for the assessment of T-cell activation and enabling researchers to make informed decisions for the creation of a protocol of their own.

Acknowledgements

This thesis marks a monumental step in my academic journey, and there are several people without whom its creation would not have been possible.

First, I want to thank Gerhard Schütz for giving me the opportunity to work and learn within the Biophysics Research Group at the Technical University of Vienna. I want to thank my supervisors Eva Sevcsik and Anežka Májková for their great guidance, kind support and constructive feedback, without which, I would not have been able to write this thesis.

Furthermore, I would like to thank Martí Romero Pons and Anna Gaugutz, who both turned out to be not only lovely colleagues but also great friends. Thank you Martí for always sharing your knowledge and thank you Anna for never failing to motivate me when the end seemed too far to reach.

I want to thank the whole Biophysics research team for always taking the time to answer my questions and support me in my work, renewing my love for science and making me feel at home from the first day on.

Lastly, I want to express my gratitude for my friends and family who have always supported me in my decisions and goals. Thank you for always being here for me.

Eidesstaatliche Erklärung

Ich erkläre an Eides statt, dass die vorliegende Arbeit nach den anerkannten Grundsätzen für wissenschaftliche Abhandlungen von mir selbstständig erstellt wurde. Alle verwendeten Hilfsmittel, insbesondere die zugrunde gelegte Literatur, sind in dieser Arbeit genannt und aufgelistet. Die aus den Quellen wörtlich entnommenen Stellen, sind als solche kenntlich gemacht. Das Thema dieser Arbeit wurde von mir bisher weder im In- noch Ausland einer Beurteilerin/einem Beurteiler zur Begutachtung in irgendeiner Form als Prüfungsarbeit vorgelegt. Diese Arbeit stimmt mit der von den Begutachterinnen/Begutachtern beurteilten Arbeit überein.

Wien, 12.03.2025

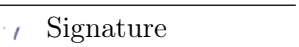

Signature

Contents

1. Introduction

T-cell activation is a complex and highly regulated process that remains a topic of ongoing investigation within the scientific community. Despite extensive research, key aspects of this process, such as the remarkable sensitivity of T-cell activation under physiological conditions, have yet to be fully recreated in-vitro. An observation that has sparked several theories about the activation process, is the reorganization of T-cell receptors (TCRs) into micro-clusters upon ligand encounter. Several studies have suggested that the pre-clustering of peptide-major histocompatibility complex (pMHC) molecules could promote this TCR reorganization and therefore facilitate T-cell activation.

Model systems are used to study biological processes, as they allow researchers to dissect individual aspects of complex processes at the molecular level, by providing a high degree of control over specific variables of the system while simultaneously simplifying it. In the context of T-cell activation, model systems offer an opportunity to recreate and manipulate specific features of the immunological synapse, thereby enabling a deeper understanding of the factors that influence T-cell activation, making them a powerful approach when trying to test this hypothesis.

Previous research by Hellmeier [1], focused on the development of a DNA origami-based model system to assess the influence of spatial parameters on T-cell activation. Specifically, the model was designed to investigate whether the spatial distance between pMHC molecules affects the activation of T-cells. To address this question, an experimental system was developed using supported lipid bilayers (SLBs) as its foundational component. SLBs serve as a mimic of the cell membrane, by forming a singular phospholipid bilayer on a solid support. By doing this, they provide a biologically relevant environment for T-cell interactions. This system is further enhanced by the incorporation of DNA origami in the form of two-dimensional platforms functionalized with pMHC molecules. These platforms introduce a high degree of controllability over spatial distances between attached molecules. By precisely positioning pMHC molecules on the DNA origami structures, it becomes possible to study the impact of spatial organization on T-cell activation.

While the combination of SLBs and DNA origami offers a promising and tunable model system for studying T-cell activation, the initial protocol lacked stability and reliability, leading to significant fluctuations in system performance. Therefore, the objective of this thesis is the optimization of the existing protocol to improve

reproducibility and functionality. To achieve this, the focus was placed on the main areas of concern, including the thermal folding process of DNA origami, the purification of folded platforms, the functionalization of DNA origami platforms, and the anchoring of platforms to SLBs. By refining these key steps, this work aims to establish a stable and reliable model system, that enables detailed studies of the impact of spatial ligand organization on T-cell activation.

2. Theoretical Background

2.1. Immunological Background

2.1.1. Principles of innate and adaptive Immune System

The immune system is a complex network of cells, tissues, and organs that defend the human body against pathogens including bacteria, viruses, or other harmful invaders. It is divided into two categories: the innate immune system and the adaptive immune system, which work together to protect the body [2].

The innate immune system is a general and non-specific defense response, that can be found in all multicellular organisms. It is designed to prevent infections, eliminate invading pathogens and activate the adaptive immune system. The innate immune system acts as the first line of defense and responds immediately to infections. It includes various mechanisms such as anatomical barriers, like the skin and mucosa, chemical defenses like antimicrobial peptides and several cellular components. Cells acting in the innate immune system include phagocytes, natural killer cells and dendritic cells. Rather than targeting specific pathogens, these cells use pathogen recognition receptors (PRRs) to recognize molecular patterns produced by pathogens. These patterns can be divided into two classes: pathogen-associated molecular patterns (PAMPs) and damage-associated molecular patterns (DAMPs). Once a pathogen is recognized, signaling pathways are activated, resulting in the initiation of phagocytosis and inflammatory responses [2–4].

The acquired or adaptive immune system is a highly specific defense response, tailored to the encountered pathogen. In comparison to the innate system, the adaptive immune system is slower in its response; however, it is capable of providing long-term immunity, known as immunological memory [5]. Vaccination is based on this principle, in which patients are injected with a weakened or inactive antigen of the pathogen, mimicking an infection. The immunological memory acquired through this process leads to a faster and more effective defense response, if the same pathogen is encountered in the future [6].

The main actors in the adaptive immune system are antigen-specific lymphocytes. They possess the ability to recognize and target pathogenetic antigens, through highly variable antigen receptors on their surface. The lymphocytes in-

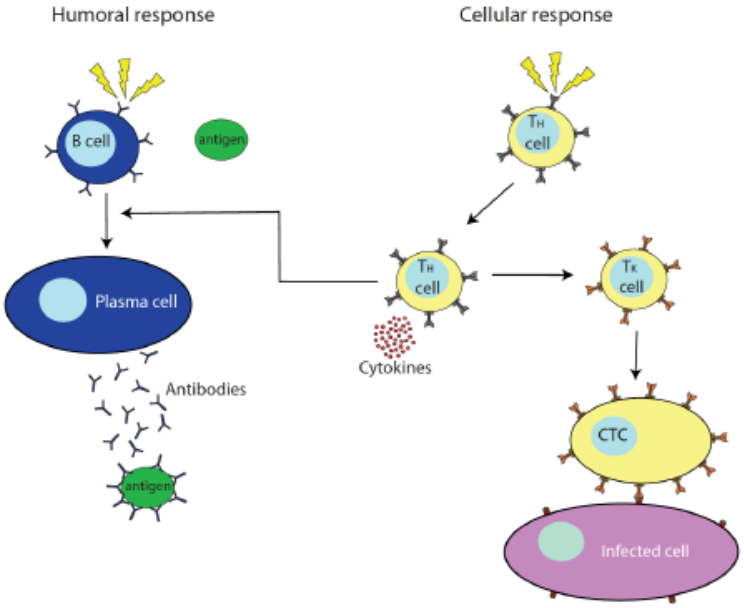

Figure 2.1.: ***Cell mediated response of the adaptive immune system.*** *Upon activation T helper (T_H) cells release cytokines to further recruit additional immune cells. The activation of both B-cells and T killer (T_K) cells strongly depend on the co-stimulation of T_H cells. Once activated, B-cells develop into plasma cells, which release antibodies to combat pathogens. T_K cells mature into cytotoxic T-cells (CTC) and directly kill infected cells. Figure taken from [1].*

volved in this process can be classified into two major subtypes, B-lymphocytes (B-cells) and T-lymphocytes (T-cells), mediating the humoral and cell-mediated immune response, respectively. Upon activation, the B-cell proliferates and differentiates into plasma cells, which produce antibodies that circulate in the bloodstream and bind to the antigens, that activated the B-cell. This results in the neutralization of the pathogen by blocking its ability to bind to host cells.

T-cells can be divided into two categories: T helper (T_H) cells, which facilitate the recruitment of additional immune cells and regulate the immune response, and T killer (T_K) cells, which directly target and destroy infected cells [5, 7]. The cells and cell reactions involved in these responses are strongly interconnected, resulting in complex pathways of immune activation. Both B- and T-cells can be activated in a number of ways, either by direct antigen recognition or through recruitment by T_H cells. A brief overview of this cellular activation process can be found in Figure 2.1.

2.1.2. T-Cell Maturation

The role of the adaptive immune system and especially T-cells is to recognize and destroy invading pathogens. Since these responses are of destructive nature, it is crucial that they are only used against foreign and harmful invaders and not against the host itself. Failure of these recognition rules could lead to possibly fatal auto-immune diseases [5]. Thus lies the great importance of the high sensitivity and specificity of T-cell activation.

T-cells are distinguished from other lymphocytes by the presence of a T-cell receptor (TCR). They can be categorized into three primary groups: T_K and T_H cells, which have been previously introduced, as well as regulatory T-cells. Regulatory T-cells function as immunosuppressors, suppressing and down-regulating the proliferation of both killer and helper T-cells, thus helping to prevent autoimmune reactions [8].

All T-cells originate from haematopoietic stem cells (HSC), which are found in the bone marrow. T-cell precursors migrate to the thymus gland to develop and fully mature into a distinct subtype. The thymus gland offers a delimited microenvironment, in which the cells undergo different levels of quality checks, leaving only a small percentage of functional cells, that are able to correctly identify foreign antigens without reacting to self antigens. This process ensures the development of functional and self-tolerant T-cells. The maturation process is divided into different stages, if any cells remain at a certain stage, they undergo apoptosis. When premature cells first arrive in the thymus gland, they express neither a TCR nor any co-receptor proteins (CD4 and CD8) and are therefore termed double-negative. In the first step of their maturation, T-cells are stimulated to express an unique TCR. After successful receptor development, cells are driven to express both CD4 and CD8 co-receptors, resulting in double-positive T-cells. In the last step, cells undergo a process of positive and negative selection, whereby cells that demonstrate excessive reactivity to self-antigens are eliminated. Cells are then directed towards a commitment of either $CD4^+$ or $CD8^+$ lineage, ultimately resulting in the formation of either a T_H cell, which expresses a CD4 co-receptor, or a T_K cell, which expresses a CD8 co-receptor. Following this process the cells are released as naive mature T-cells into the bloodstream [7].

2.1.3. T-Cell Activation

To enable the recognition of an antigen, it must be bound to a major histocompatibility complex (MHC) molecule in the form of a peptide-loaded major histocompatibility complex (pMHC) (see Fig. 2.2). MHC molecules are divided into two classes: MHC-I and MHC-II. MHC-I is expressed on the cell membrane of virtually all nucleated cells within the body. It is recognized by T_K cells, which

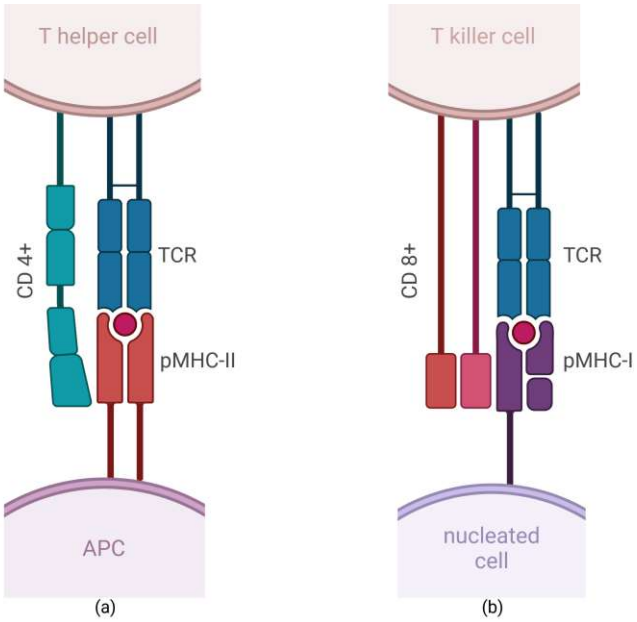

Figure 2.2.: ***TCR:pMHC binding.*** ***(a)*** *Binding of a T helper (T_H) cell to a major histocompatibility complex class two (MHC-II) with the help of its co-receptor CD4.* ***(b)*** *Binding of a T killer (T_K) cell to a MHC class one (MHC-I) with the help of its co-receptor CD8. Both CD4 and CD8 enable a stable TCR:MHC binding and help the T-cell to correctly identify the encountered MHC molecule. Created with BioRender.com*

form a stable TCR-MHC complex with the help of their CD8 co-receptor. MHC-I presents intracellular antigens to the T_K cell. Under physiological conditions, the antigen presented is a self antigen, however, in the case of infection or mutation of the cell, viral particles or tumor-specific antigens are presented by the pMHC. The interacting T_K cells are able to recognize and respond to these pathogenic antigen peptides. In contrast, MHC-II is exclusively expressed on antigen presenting cells (APCs), and its function is to present extracellular pathogens that have undergone phagocytosis as peptide fragments to T_H cells, which, once an extracellular pathogen is recognized, activates and recruits B- and T_K cells to combat the harmful invader [9].

While this activation process seems to be straightforward, two major questions still remain. It has yet to be understood how the T-cell discriminates between self- and agonist peptides and how the successful recognition of a harmful peptide is then translated into an intracellular signal. For both these questions, several hypotheses have been proposed [10–13], yet no consensus has been reached. This gap in knowledge still persists, due to the difficulties of observing such a highly

dynamic and complex process without disrupting it.

Furthermore, the spatial arrangement of both pMHCs and TCRs has been theorized to play a key role in the activation process [14, 15]. It has been observed that, upon ligand encounter, TCRs reorganize into microclusters [16, 17], yet there is no consensus as to whether pre-clustered ligands can promote TCR clustering and therefore facilitate the activation of T-cells [18–20]. In order to test this, the clustering of pMHC is imitated with the help of DNA origami platforms, that allow for the precise control of ligand spacing at the nanometer scale.

2.2. Nanotechnological Background

2.2.1. DNA - biological and historical Background

DNA as nature's information carrier is one of the most famous molecules of modern biology. First imaged through X-ray crystallography by Rosalind Franklin in 1953, it's distinct double-helical shape was soon after discovered, initiating a deeper understanding of not only how the molecule was constructed but what it was capable of. Today we know that the DNA holds the genetic information needed for development, growth and reproduction of every living being as well as many viruses [21].

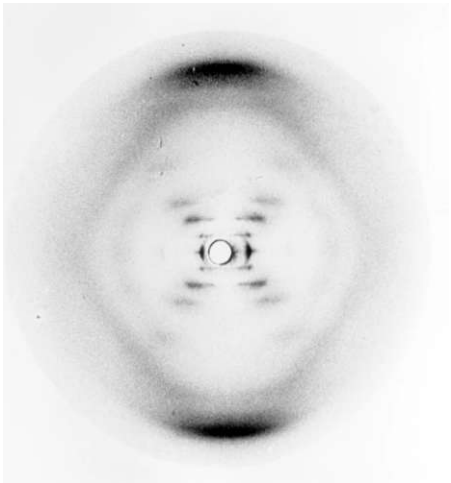

Figure 2.3.: ***First image of the DNA***. *In 1953 Rosalind Franklin took the first images of the DNA via X-ray crystallography leading to the discovery of it's helical shape. Image taken from [22].*

Deoxyribonucleic acid (DNA) is a nucleic acid, one of four molecule classes (lipids, proteins, carbohydrates and nucleic acids) that are the major building

blocks of the human body. It consists of two polynucleotide chains that are twisted around each other to form a double helix [23].

Each polynucleotide chain is composed of repeating monomeric units called nucleotides, which are themselves composed of three major components: A phosphate group, a pentose sugar (deoxyribose) and a nitrogenous base (depicted in Fig. 2.4a). DNA contains four different bases, two purine (adenine and guanine) and two pyrimidyne bases (cytosine and thymine), which form the core of the information transfer capabilities of DNA.

One phosphate group links the sugars of two nucleotides, thereby forming a sugar-phosphate backbone. The ends of these single stranded DNA (ssDNA) strands differ from one another. One end contains a 5´ phosphate group, while the other end contains a 3´ hydroxyl group. This end configuration gives the ssDNA a distinct directionality, with the 5´ end being the primer end and the 3´ end being the non-primer end [21]. Two ssDNA strands invariably form an antiparallel bond through their bases via hydrogen bonds (Fig. 2.4b). The binding of these bases is not a random process; rather, base pairs are constructed that are exclusively capable of binding with each other. The rules of base-pair binding in DNA, also known as "Watson-Crick" base pairing, dictate that adenine always binds to thymine and guanine always binds to cytosine. This rule subsequently leads to the complementary relationship between two ssDNA strands as well as the ability to multiply DNA. The structure of one ssDNA strand provides immediate knowledge about the structure of its counterpart [24]. This characteristic also forms the basis for the use of DNA as a nanotechnological tool.

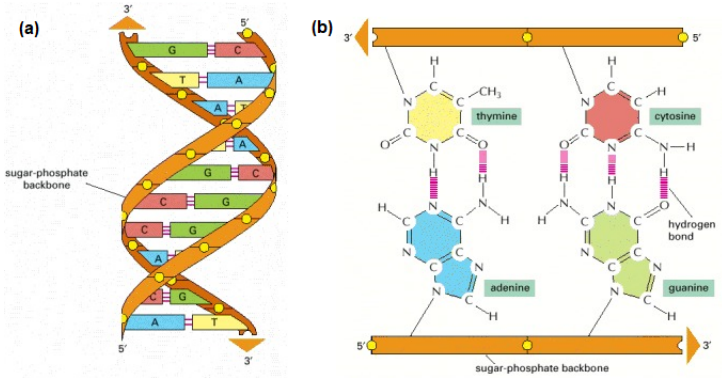

Figure 2.4.: ***Structure of the DNA.*** ***(a)*** *Two single stranded deoxyribonucleic acid (ssDNA) strands form the typical double helix of the DNA.* ***(b)*** *Two complementary ssDNA strands bind to each other via hydrogen bonds of the corresponding bases (A-T and G-C). Images adapted from [5].*

2.2.2. Nanotechnological Use of DNA

As defined by the Encyclopædia Britannica, nanotechnology is "the manipulation and manufacture of materials and devices on the scale of atoms or small groups of atoms" [25]. Two distinct approaches are commonly employed within this field. The "top-down" approach involves the reduction of larger structures to the nanoscale, a process that can become increasingly challenging as the desired structure becomes smaller. In contrast, the "bottom-up" approach utilizes information within molecules to assemble them into nanostructures [26]. It is therefore not farfetched to utilize biological systems, such as cell membranes, nucleic acids or proteins, which have been optimized through evolution over eons, as working materials for "bottom-up" approaches. In nanotechnology, DNA is taken out of its biological context, using the molecule as a building block rather than an information carrier. This is made possible by the predictable nature of "Watson-Crick" base pairing and the resulting assembly of two ssDNA strands. By understanding the specific binding patterns between adenine and thymine and guanine and cytosine, DNA can be guided into pre-designed nanostructures through self-assembly [26].

First to utilize this feature was biophysicist Nadrian Seeman [27], who in the 1980s developed a technique to force DNA into branched junctions through base pairing, enabling macromolecule arrangement into 3D crystal formations. And even though this technique marks a turning point in the DNA nanotechnological field, it still had drawbacks in the terms of flexibility and stability [26]. The next major milestone was presented by Paul Rothemund [28], who in 2006 publicized a novel technique of creating nanostructures out of DNA, called DNA origami. Rothemund's method uses a long, singular strand of DNA, called the scaffold and forces it into a desired shape with the help of many short strands of DNA, called staple strands. A major advantage of this technique is its comparably easy one-pot folding method. Rothemund showed that DNA origami can be utilized to create a variety of different structures, ranging from simple rectangles up to stars and smiley faces [28]. DNA origami not only provides a way of creating 2D shapes, soon after the publication of Rothemund's paper, several research teams showed the possible extension into the three dimensional space [29–31].

The full potential of DNA origami, however, lies in its functionalization, given that DNA itself lacks active chemical, electrical or optical functionalities, and its programmability. The addition of DNA-tagged, functional components, such as proteins or fluorophores, to DNA origami structures can be achieved, through hybridization with excess bases of selected staple strands, that protrude from the structure (see Fig. 2.6b). This addition can be realized in a highly organized manner, with nanometer precision and control over the exact number, orientation and position of the incorporated units [32, 33].

2.2.3. Supported Lipid Bilayers

Supported lipid bilayers (SLBs) are a commonly used method to mimic cell membranes. They consist of a lipid bilayer supported on a solid substrate like glass, silica or mica. Their simplicity and controllability make them a valuable tool for studying biological processes and membrane biophysics like signaling mechanisms, ion transport or various intra- and extracellular processes [34]. These bilayers not only allow an easy integration of molecules relevant to signaling [35], they are also compatible with a wide range of surface sensitive measurement techniques, including fluorescence microscopy techniques [36].

Typically, phospholipids, like 1-palmitoyl-2-oleoyl-sn-glycero-3-phosphocholine (POPC) (see Fig. 2.5a), are used in this application, as they are the primary components of cell membranes and can spontaneously form bilayers as they orient in aqueous solutions in such a way that their hydrophilic heads face outward while their hydrophobic tails are oriented inward. Additionally, the mobility of proteins attached to an SLB created with POPC is comparable to a physiological plasma membrane. SLBs are typically formed from small unilamellar vesicles (SUVs), which are prepared by sonicating or extruding lipid mixtures. These vesicles are then introduced to a solid, hydrohphilic surface, such as glass. Due to a combination of van der Waals attractions, electrostatic interactions and hydration forces the vesicles get adsorbed onto this surface. Surface forces lead to stress and consequent deformation of SUVs, followed by the fusion of several vesicles. Once the stress exceeds a threshold, the vesicles rupture and the SLB is formed by lateral spreading (Fig.2.5c). Other methods for SLB formation include Langmuir-Blodgett deposition and spin-coating, but vesicle fusion remains the most commonly employed due to its simplicity and effectiveness [34, 37–39].

An important characteristic of SLBs is their lateral mobility, which refers to the ability of lipid molecules to diffuse laterally within the plane of the bilayer, due to a layer of water molecules between the solid and the bottom layer of the lipid bilayer (Fig. 2.5b). The lateral diffusion of lipids in SLBs is influenced by several factors, including lipid composition, substrate type, and the presence of additives such as cholesterol [40].

As the creation of a flawless SLB cannot be guaranteed, a method of reducing errors, such as holes, is the use of bovine serum albumin (BSA). This protein can be used to passivate hydrophilic surfaces, thus preventing the non-specific adhesion of later added surface proteins onto the solid support and ensuring the correct incorporation into the SLB [41].

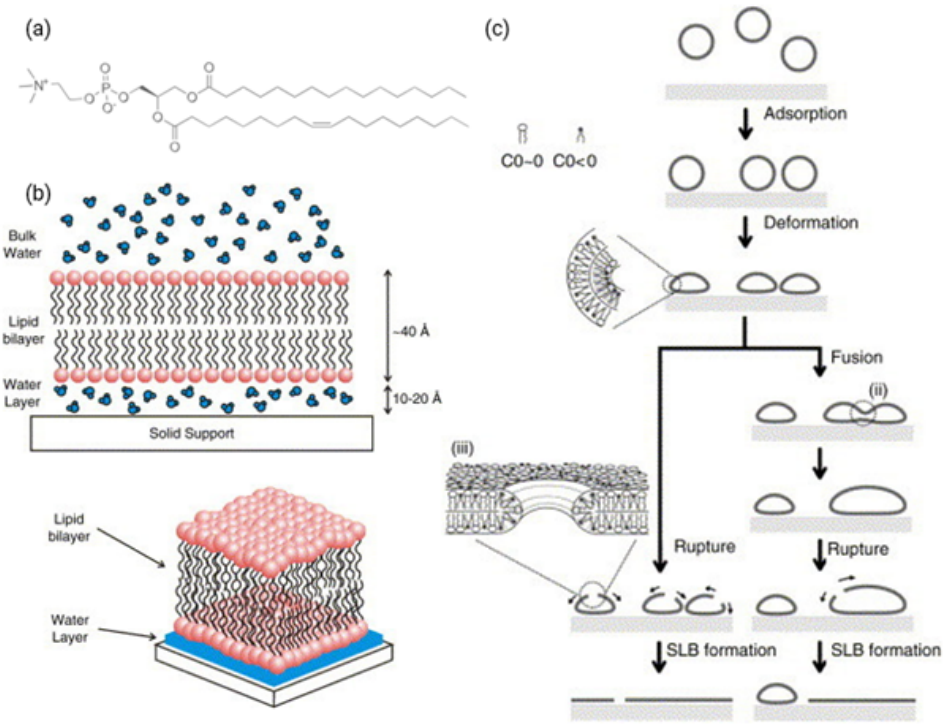

Figure 2.5.: ***Supported Lipid Bilayer (SLB).*** ***(a)*** *Chemical structure of POPC.* ***(b)*** *Planar lipid bilayer on a solid support (e.g. glass or mica). A thin water layer between the solid surface and the bottom layer of the lipid bilayer leads to lateral mobility of the SLB.* ***(c)*** *SLB formation via vesicle fusion. Small unilamellar vesicles adsorb onto an hydrophilic surface. Surface forces lead to deformation and consequent rupture of the vesicles, resulting in the spreading of the bilayer onto the surface. Images taken from [38, 39, 42]*

2.3. Model System Creation to investigate T-Cell Activation

Model systems are a convenient method to study certain biological mechanisms, as they allow precise control over experimental conditions, enabling researchers to dissect specific aspects of biological processes at the molecular level. The system used in this work, is based on two major components, SLB, mimicking the fluidity and mobility of an APC and DNA origami platforms, which enable controllability over the spatial arrangement of signaling molecules. Thus, the model system created allows for the significance of the spatial distribution of pMHC ligands in T-cell activation to be investigated.

2.3.1. Design of DNA Origami

When designing a DNA origami structure, its intended purpose has to be carefully considered. In the model system used in this project, the DNA origami serves as a tool to control the spatial distribution of pMHC ligands. For this application, a 2D platform measuring 70 nm x 100 nm was sufficient. The design process begins by creating a geometric model of the DNA origami layout, which involves taking a long viral scaffold ssDNA strand and folding it into the desired shape. Short staple strands are then strategically placed to stabilize the structure in the desired form (Fig. 2.6a) [28]. Staple strands must be added in accordance with a certain set of rules. To simplify this process, *CaDNAno* [43], a computer-aided design (CAD) software, can be used. This software offers a range of tools that simplify and accelerate the design process through features such as automated staple routing, adequate alignment of staple strands with the scaffold strand as well as additional editing tools.

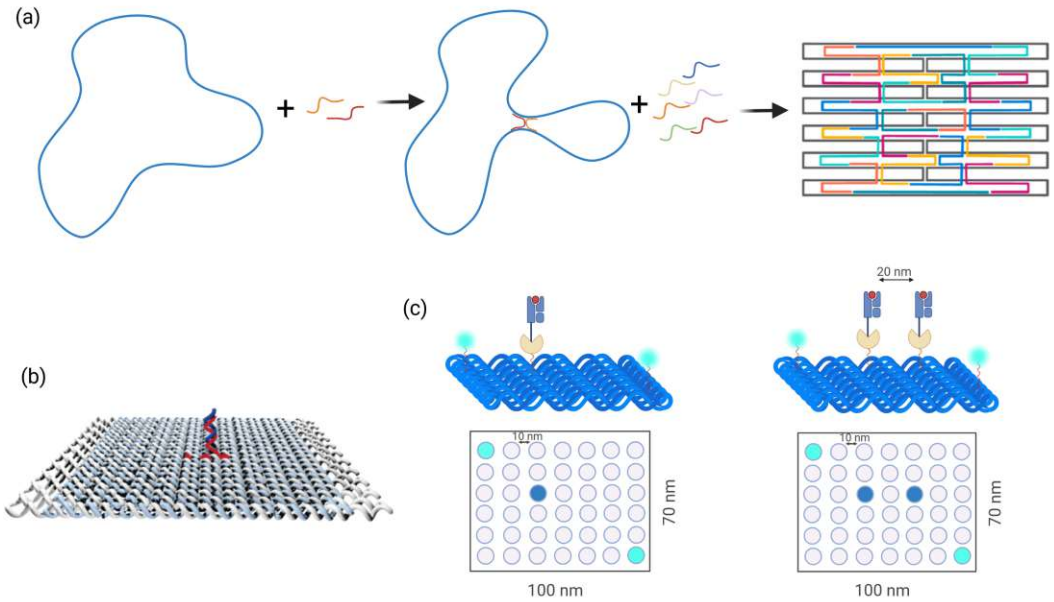

Figure 2.6.: ***Design of DNA origami platform.*** ***(a)*** *A long singular scaffold strand is forced into a predesigned shape by small staple strands.* ***(b)*** *DNA platform with a modification site allowing the addition of functional modifications like fluorophores, ligands, etc. Image taken from [1].* ***(c)*** *Possible modification sites on the platform allow the precise addition of different functional modification at fixed distances. Figure partially created with BioRender.com*

The platform used in this work was pre-designed [1] and includes multiple modification sites that allow the integration of ligands, fluorophores, or other functional components at specific locations (see Fig. 2.6c). These modifications are implemented by adding staple strands with protruding extensions to the DNA origami structure (Fig. 2.6b). These extensions can hybridize with complementary strands, enabling modifications to be introduced either directly during the folding process or afterward by incubating the folded DNA origami with the desired modification [1]. To ensure sufficient attachment, the extensions must be at least 16 base pairs long. This length provides adequate stability for hybridization and subsequent functionalization [44].

2.3.2. Folding and Purifying of DNA Origami

A significant appeal of DNA origami over other nanontechnologies is its simple self-assembly. This process is a one-pot method and involves mixing the scaffold strand, staple strands, and optional modifications into an appropriate folding buffer solution, followed by subjecting it to a thermal folding protocol. Staple strands are added at a molar excess of at least $10x$ to ensure the correct folding of the nanostructures [28, 45, 46]. The exact folding protocol is dependent on the complexity and design of the nanostructure. The folding process is typically performed in a thermocycler. As a first step, the mixture is heated to a peak temperature between 60°C and 90°C in order to disassociate any aggregated or entangled DNA. To prevent possible damage to the DNA, the peak temperature is only held briefly, before the mixture is then cooled slowly in a stepwise manner, allowing the DNA to fold into the desired DNA origami structure [28, 47]. The effectiveness of the chosen folding protocol is validated by assessing the quality of the folded DNA origami structures using agarose gel electrophoresis, which separates correctly folded structures from misfolded ones and unused staple strands [47].

Several methods are available to purify DNA origami, with the choice of method depending on the form of the nanostructure as well as modifications that may have been introduced. Two common purification techniques are ultra-filtration and agarose gel electrophoresis [48].

Ultra-filtration involves passing the DNA origami solution through a membrane with a molecular weight cut-off, typically 100 kDa or higher, depending on the nanostructure. The filtration tube is centrifuged to force the solution through the membrane, which retains the larger DNA origami structures while allowing smaller molecules like excess staple strands to pass through. This method is time-efficient, scalable, and offers relatively high recovery yields. However, it does not separate aggregates or misfolded structures from correctly folded DNA origami [48].

Agarose gel electrophoresis separates DNA origami structures based on size and charge. The sample is loaded into wells of an agarose gel, before applying an

electric field. DNA molecules migrate through the gel matrix toward the positive electrode, with their mobility being determined by size and shape. As DNA origami structures are larger and more complex than excess staples or other small contaminants, they migrate more slowly, allowing separation. Following the separation process, the purified sample has to be first mechanically removed from the rest of the gel setup, before extraction. This method produces highly purified samples, as it removes not only excess staple strands but also aggregates and misfolded structures. However, the process is time-consuming and labor-intensive, and often results in low recovery yields [48–50].

2.3.3. Platform Functionalization with pMHC

In order to utilize the DNA origami platforms as intended, they have to be functionalized with pMHC. A key requirement for this functionalization is ensuring a close resemblance to the surface of an APC. This involves maintaining a degree of flexibility in the movement of the ligands to accurately mimic the physiological contact between a T_H cell and an APC. To achieve the simultaneous restriction and flexibility in ligand movement, the chosen DNA origami construct (the efficiency of which has been demonstrated in previous works [1, 51]), consists of two distinct parts.

pMHC is bound to the platforms via streptavidin:biotin binding. Streptavidin, a protein produced by *Streptomyces avidinii*, has four distinct biotin-binding sites and forms one of the strongest known non-covalent interactions in nature [52, 53]. In order to create an operational complex, streptavidin is modified to create monovalent streptavidin (mSA), where three of its four binding sites are inactivated, leaving only one functional biotin-binding site. This ensures controlled binding and reduces potential complications from multivalency [54, 55]. The mSA is further modified by attaching an oligonucleotide, to allow hybridization with the DNA origami platform.

Subsequently, biotinylated pMHC is introduced into the system. The biotin moiety exhibits a strong binding affinity for mSA, allowing the use of relatively long biotin linkers without risk of detachment, thereby enabling the pMHC to retain the flexibility required to mimic physiological TCR:pMHC interactions. This design replicates natural interactions with sufficient accuracy to facilitate T-cell activation [55].

2.3.4. Platform Anchoring

The overall goal of this step, is to anchor DNA origami platforms to an SLB in a way, that preserves their mobility, since under physiological conditions, ligands can diffuse freely on the surface of APCs, thus making this a crucial aspect for

successful T-cell activation.

When anchoring a DNA origami platform to a SLB, electrostatic interactions between the two have to be carefully considered. Nucleic acids, such as DNA, are highly negatively charged, while zwitterionic lipids, such as POPC, have no net charge. However, there can still be local charge imbalances or dipoles on the lipid bilayer surface. Magnesium chloride ($MgCl_2$) is commonly used to facilitate the attachement of nanostructures through a phenomena called cation bridging. The Mg^{2+} ions have a strong affinity for binding to the phosphate groups in DNA, neutralizing their negative charges and allowing interaction with the SLB. Additionally, the dipoles of the zwitterionic lipids can stabilize the binding via Mg^{2+} coordination. Although zwitterionic bilayers are charge-neutral overall, these weak interactions mediated by Mg^{2+} provide sufficient stability for attachment [56, 57]. A limitation of this method is its non-specificity, as the proper orientation of the DNA origami platform cannot be assured.

Cholesterol-modified oligonucleotide anchors can offer an effective solution for attaching DNA platforms to SLBs [58]. In this method, cholesterol-modified DNA strands are designed to carry a specific sequence complementary to one located at the base of the DNA platform. The strong hydrophobic nature of cholesterol results in a robust interaction with the hydrophobic tails of POPC lipids, firmly anchoring the platform to the SLB. The binding strength can be adjusted by the number of cholesterol anchors per platform. A significant advantage of this method is the ability to control the orientation of the DNA platforms relative to the SLB [59, 60].

2.3.5. SLB Modification

Apart from anchoring functionalized DNA origami platforms to them, SLBs can be functionalized in order to closely mimic the surface of APCs, using various strategies. One effective approach involves the binding of polyhistidine- (His-) tagged proteins directly to lipids such as 1,2-dioleoyl-sn-glycero-3-[(N-(5-amino-1-carboxypentyl)iminodiacetic acid)succinyl](nickle salt) (DGS-NTA(Ni)). This method enables the incorporation of essential co-stimulatory and cell adhesion proteins (e.g., intercellular adhesion molecule (ICAM) and B7) into the SLB. These functionalized SLBs allow for the free diffusion of the proteins across the bilayer surface, facilitating the reorganization and formation of micro- and nano-scale clusters during interactions with T-cells [1] (see Fig.2.7).

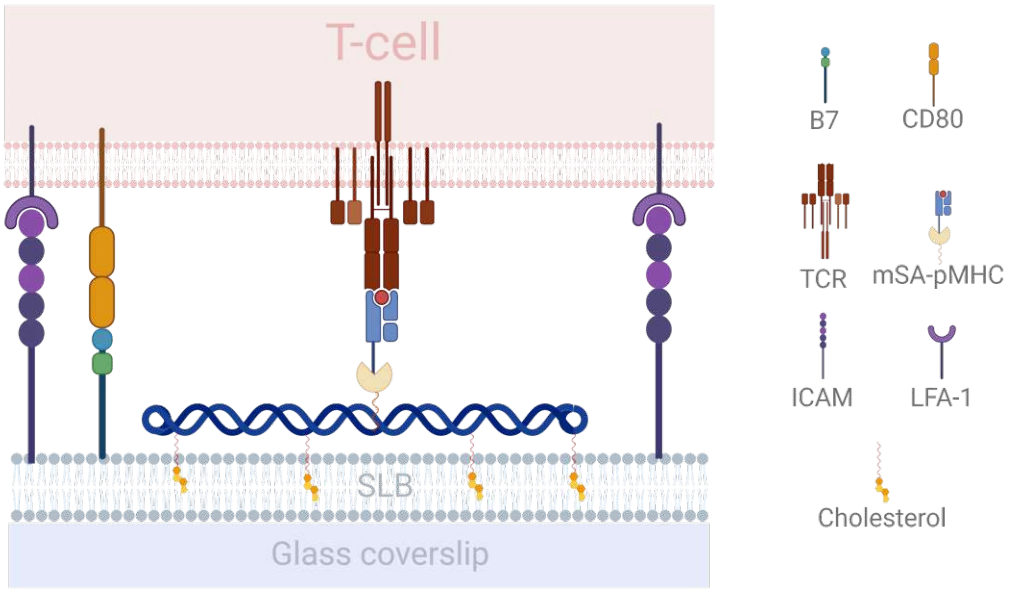

Figure 2.7.: ***Model System to investigate T-cell activation.*** *A DNA origami platform is anchored to a supported lipid bilayer (SLB) via cholesterol strands. Platforms carry peptide-loaded major histocompatibility complex (pMHC) molecules, attached via molovalent strepdavidin (mSA). Co-stimulatory molecules (B7) and cell adhesion molecules (ICAM) are added directly to the SLB via HIS-tags. Created with BioRender.com*

2.4. Total Internal Reflection Fluorescence Microscopy

Total internal reflection fluorescence (TIRF) microscopy is a type of fluorescence microscopy, that enables the imaging of a thin layer in an aqueous or cellular environment, in close proximity to a solid surface, without exciting regions further away. Employing this technique results in images that exhibit a high signal-to-noise ratio and almost no out-of-focus fluorescence. It is therefore popular for the visualization of, among others, membrane structures and single cell dynamics as well as the tracking of singular molecules near a surface [61].

TIRF microscopy is based on the principle of total internal reflection (TIR) of a light beam that hits the interface of two media with different refractive indices. If the beam propagates from a medium with a high refractive index to one with a low refractive index, rather than being refracted through the interface, it will undergo TIR, if the angle of the incident light beam exceeds a critical value θ_c (see Figure 2.8). The refractive behavior of a light beam is given by Snell's law (Eq. 2.1),

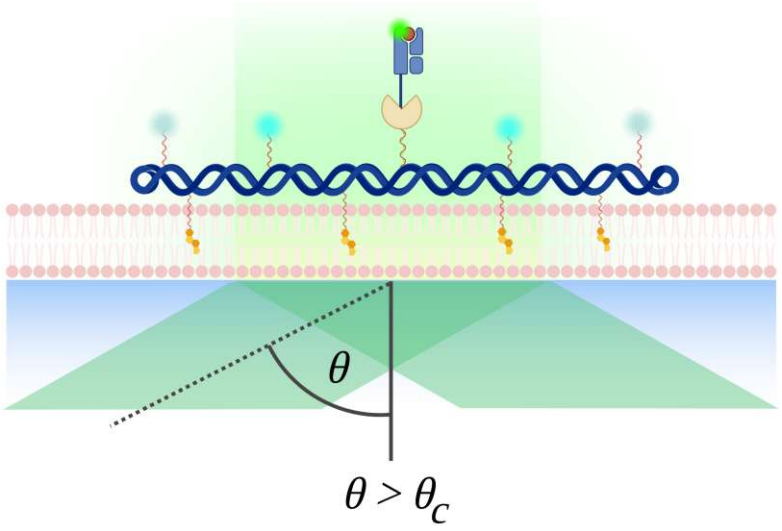

Figure 2.8.: ***TIRF Microscopy.*** *A light beam is totally reflected at the interface between two media with differing refractive indices, if it propagates from a medium with high refraction to one with low refraction and the incident angle θ is greater than a critical angle θ_C. Consequently, an electromagnetic field of around 100 nm thickness is produced, which is capable of exciting fluorophores within this distance. Created with BioRender.com*

where n_1 and n_2 refer to the refractive indices of two media and θ_1 and θ_2 to the angels of the incident and refracted light beams with respect to the normal to the interface. With the assumption of n_1 representing the medium of higher index of refraction, and knowing that at the critical incident angle θ_c the refraction angle θ_2 is 90, we get Equation 2.2.

$$sin(\theta_1) \cdot n_1 = sin(\theta_2) \cdot n_2 \tag{2.1}$$

$$sin(\theta_c) \cdot n_1 = n_2 \tag{2.2}$$

converted to θ_c :

$$\theta_c = sin_{-1}\left(\frac{n_2}{n_1}\right), n_1 > n_2 \tag{2.3}$$

If TIR occurs, a highly restricted electromagnetic field with a frequency identical to the incident beam is generated in the medium of lower refractive index. This field decays exponentially with distance to the interface, while simultaneously being able to excite fluorophores. This results in an excitable region of around 100 nm from the surface [62].

3. Material and Methods

3.1. DNA Origami

In order to establish a protocol that ensures stable and reproducible results, the individual steps in the protocol were examined and modified as necessary. The following provides an overview of the entire protocol, highlighting the steps that were tested. All experiments were conducted using pre-designed DNA origami platforms with a size of 70 nm x 100 nm. For further information on the platforms, see [1].

3.1.1. Folding of DNA Origami

DNA origami platforms were created in a single one-pot folding reaction carried out in a polymerase chain reaction (PCR) tube (Bio-Rad Laboratories), each containing DNA origami mixture (ssDNA scaffold type p7249 (tilibit nanosystems GmbH), a mixture of single stranded staple strands (Microsynth AG)), together with 10 µl folding buffer (FoB) (50 mM Tris (ThermoFisher Scientific™), 500 mM NaCl (ThermoFisher Scientific™), 10 mM EDTA (ThermoFisher Scientific™)), 12.5 mM $MgCl_2$ and optionally fluorophore-modified strands (Microsynth AG) (for detailed origami mixtures see Tables A.1 - A.4).

3.1.1.1. Variations in Thermal Folding Protocol

In an effort to find a thermal folding protocol that ensures an optimal trade-off between platform quality and folding time, three different folding protocols were created and tested (see Table 3.1). The platforms were annealed using one of these three protocols.

3.1.1.2. Quality Control

The quality of the resulting DNA origami platforms was investigated via agarose gel electrophoresis. An in depth description of the process can be found in Chapter 3.1.2.1. Testing of folding protocols was done in the course of other experiments, and never as a stand-alone.

Table 3.1.: **Tested thermal folding protocol variations.** Three different folding protocols were tested to investigate the influence of the starting temperature as well as the cooling rate of the protocol on the quality of the folded DNA origami platforms.

Protocol	1 min	10 min	60 min
Start Temperature	90°C	75°C	75°C
Holding Time [min]	15	15	-
Cooling Pace [°C/min]	1	1/10	1/60
End Temperature	4°C	4°C	4°C

3.1.2. DNA Origami Purification

As the yield of correctly folded DNA origami platforms can never be 100 %, the samples have to be purified to remove of excess staple strands and improperly folded structures. Two different methods were compared in terms of time efficiency, labor intensity, and recovery yield. The effectiveness of both methodologies was evaluated through diffusion measurements, assuming that the presence of residual aggregated platforms in inadequately purified DNA origami would result in lower diffusion values.

3.1.2.1. Agarose Gel Electrophoresis

The folded DNA origami platforms were mixed with 1 % DNA Gel Loading Dye (Thermo Scientific™) relative to the sample volume, before being exposed to agarose gel electrophoresis (1x Tris Acetate-EDTA (ThermoFisher Scientific™), 10 mM $MgCl_2$, 1.5 % agarose (Carl Roth GmbH), 6.6 % 10x SYBR™ Safe DNA Gel Stain (ThermoFisher Scientific™)). 5 µl of GeneRuler 1 kb DNA Ladder (Thermo Scientific™) were added as a reference. To prevent overheating the purification was carried out on ice at 65 V for 90 min. Agarose gels were visualized using a trans-illuminator (Thermo Fischer Scientific™). The sample is split up according to the size and charge of its individual parts. The smaller and more charged, the faster a molecule is transported through the gel. The resulting bands give a clear distinction between unused staple strands, correctly folded platforms and incorrectly folded platforms. The band containing correctly folded platforms were cut out using a scalpel. Two different extraction methods were applied during the course of the experiments. In the first method, the platforms were extracted manually by pressing the isolated band between two surfaces and collecting the liquid with a pipette. In the second method, the band was loaded into Freeze 'N Squeeze™ DNA Gel Extraction Spin Columns (Bio-Rad Laboratories). The columns were then incubated at -20°C for 15 min, before being centrifuged at 13000x g for 3 min

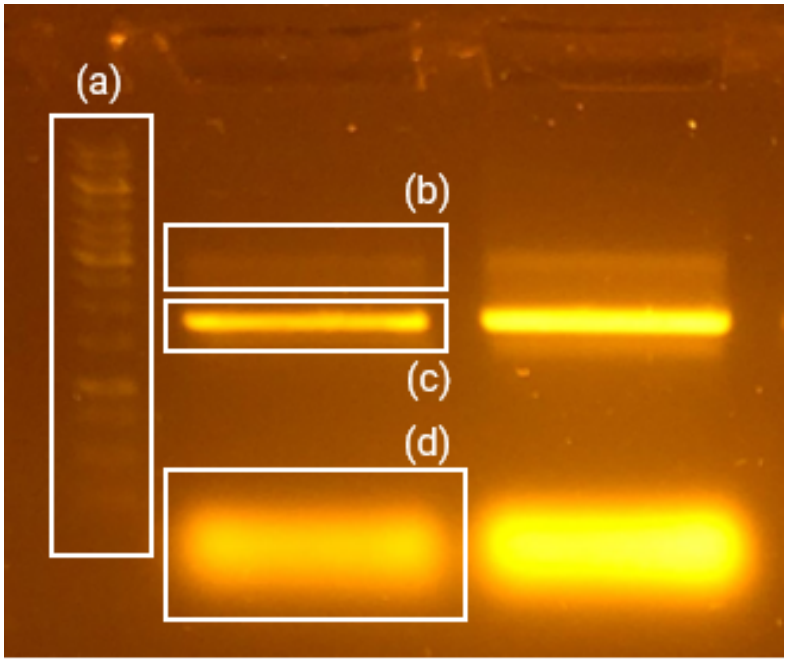

Figure 3.1.: ***DNA origami platforms purified via argaroge gel electrophoresis.*** ***(a)*** *DNA ladder,* ***(b)*** *aggregated and misfolded DNA origami platforms,* ***(c)*** *correctly folded DNA origami platforms,* ***(d)*** *excess staple strands*

at 4°C. The extracted platform concentrations were measured using a microplate reader (BioTek Synergy H1). The sample was transferred to an Eppendorf 1.5 mL Biopur® (Sigma-Aldrich) tube and stored at -20°C.

3.1.2.2. Ultra-Filtration

100 kDa Amicon®Ultra 0.5 mL centrifugal filters (Merck) were pre-rinsed by loading them with 500 µL purification buffer (PuB) (5 mM Tris, 50 mM NaCl, 1 mM EDTA, 10 mM $MgCl_2$) and centrifuging at 5000x *g* for 5 min at room temperature. The flow through was discarded of, filters were refilled with the sample and if necessary filled up to 500 µL using PuB. To purify the sample the 100 kDa Amicon®Ultra centrifugal filters were centrifuged at 7000x *g* for 5 min at room temperature. After discarding of the flow through the filters were again filled up with PuB and centrifuged. In total the sample was purified three times following the mentioned steps. For recovery the filter were inverted into a fresh tube containing 20 µL PuB and spun at 5000x *g* for 4 min at room temperature. The platform concentrations were measured using a microplate reader. The sample was transferred to an Eppendorf 1.5 mL Biopur® tube and stored at -20°C.

3.1.3. DNA Origami Functionalization

Thawed DNA origami was incubated with a 3x molar excess of mSA (c = 0.37 mg/mL) (provided by René Platzer, Medical University of Vienna) for 60 min at room temperature. Unbound mSA was removed via ultra-filtration at 4°C. 100 kDa Amicon®Ultra 0.5 mL centrifugal filters were pre-rinsed by loading them with 0.5 mL PuB and centrifuging at 4000x *g* for 10 min at 4°C. After discarding of the flow through the filters were filled with the sample and if necessary filled up to 0.5 mL using PuB. The sample was then purified by centrifuging at 4000x *g* for 15 min at 4°C. After discarding of the flow through the filters were again filled up to 0.5 mL and the purification step was repeated. The purified sample was collected by inverting the filter into a fresh tube containing 20 µL of PuB and spinning at 2000x *g* for 4 min at 4°C. Volume and concentration was measured. DNA origami functionalized with mSA was mixed with fluorescently labeled pMHC (c = 0.265 mg/mL) (provided by René Platzer, Medical University of Vienna) in an 1:5 molar ratio and incubated for 60 min.

3.1.3.1. Variations in DNA Origami Functionalization

The protocol was evaluated in two specific aspects in order to assess its effectiveness. To investigate whether the quality of the DNA origami:mSA construct was influenced by the preparation time, three protocol variations were compared. In the first variation, the incubation with mSA was performed one day in advance and stored at -20°C, rather than directly on the day of measurement, as was done in variation two. In the last protocol variation, mSA and pMHC were mixed directly with the DNA origami platforms on the day of measurement in molar ratios of 1:3 and 1:5, respectively. The sample was not purified via ultra-filtration, but used directly in the model system. Variations one and two were further investigated to determine if incubation temperature affected mSA binding efficiency. Platforms were incubated with mSA at 37°C and compared to those incubated at room temperature. Both protocol variations were analyzed in regard to the efficiency with which proteins were bound to DNA origami platforms. The results were evaluated by co-localization measurements (see Chapter 3.2.3) to determine the effectiveness of the binding process.

3.1.4. SLB Production

3.1.4.1. Vesicle Formation

The vesicle solution was prepared using POPC (Avanti® Polar Lipids, Inc.) and DGS-NTA(Ni) (Avanti® Polar Lipids, Inc.). The lipids were combined in a ratio of 98 % POPC and 2 % DGS-NTA(Ni). To achieve a 1x vesicle solution, lipids

were pipetted in a concentration of 125 µM into a glass phiole and put under a constant N_2 flow for 20 min, in order to remove residual chloroform. The lipids were diluted in 1 mL 10x Dulbecco's phosphate buffered saline (DPBS) (Sigma-Aldrich) using a Vortex mixer (IKA Labortechnik). The sample was sealed using Parafilm® (Amcor Limited) and vesicles were formed via sonication (Emmi®-D40, EMAG Technologies®) for 10 min at room temperature. The vesicles were stored at 4°C until further use, but for a maximum of 24 hours.

3.1.4.2. Bilayer Formation

The SLBs were created in a Nunc™ Lab-Tek 8-well chamber (LTC) (Thermo Scientific™) on a glass cover slip. The cover slip was first cleaned using a plasma cleaner (Harrick Plasma) for 2 min at room temperature. This ensured a hydrophilic surface, necessary for the bilayer creation. The existing glass bottom was removed from the LTC and the cleaned glass cover slip was fixed to it with eco-sil extrahart addition-curing duplicating silicone (Picodent). After letting the adhesive dry for 10 min at room temperature, 200 µL of vesicle solution were pipetted into each well.

3.1.5. SLB Functionalization

In order to functionalize the SLB, it is first incubated with cholesterol-modified DNA strands, which, due to their hydrophobicity, incorporate into the bilayer. In a subsequent step, the platforms, which bear complementary DNA strands at their base, are introduced to the system. These platforms hybridize with the cholesterol strands, thereby anchoring them to the SLB. Two different SLB functionalization protocols were tested to achieve samples with stable and reproducible surface density values.

3.1.5.1. SLB Functionalization without $MgCl_2$

The vesicles were incubated for 20 min at room temperature. Afterwards, each well was thoroughly washed using 25 mL 1x DPBS. To ensure the same volume (450 µL) in each well, the meniscus as well as 330 µL were removed. This was done after each washing step. 100 nM cholesterol-TEG-Z, complementary to oligonucleotides at the bottom of the platforms, were diluted in 49.5 µL 1x DPBS and added to each well. Cholesterol-DNA was incubated for 60 min at room temperature. After incubation each well was washed with 25 mL 1x DPBS + 0.1 % BSA (Sigma-Aldrich) to passivate the coverslips to ensure a more homogeneous bilayer. DNA origami platforms were pipetted in chosen concentrations into the wells. The chamber was covered with aluminium foil to protect from photobleaching and

incubated for 60 min at room temperature. After incubation each well was washed using 25 mL 1x DPBS.

3.1.5.2. SLB Functionalization with $MgCl_2$

The $MgCl_2$ mediated SLB functionalization was adapted from Hu et al. [63]. The vesicles were incubated for 15 min at room temperature. Afterwards, each well was washed with 0.025 mL BSA (0.1 %) diluted in 25 mL 1x DPBS, to passivate the SLB. The meniscus as well as 330 µL were removed. After incubating for 30 min at room temperature, 100 nM cholesterol-TEG-Z (biomers.net), complementary to oligonucleotides at the bottom of the platforms, diluted in 99.5 µL 1x DPBS were added to each well. The chamber was incubated for 15 min at room temperature, before washing each well thoroughly with 10 mM $MgCl_2$ diluted in 25 mL 1x DPBS. DNA origami platforms in chosen concentrations and diluted in a 10 mM $MgCl_2$ 1x DPBS solution were added to each well. The LTC was covered in aluminium foil and incubated for 60 min at room temperature. Afterwards each well was washed using 10 mM $MgCl_2$ diluted in 25 mL 1x DPBS.

3.2. TIRF Microscopy Imaging

Surface density and diffusion of the DNA origami platforms as well as co-localization measurements were obtained using a TIRF microscope. The system in use was home built and based on a Zeiss Axio Observer 7 microscope. The setup was equipped with an α plan-apochromat objective (100x/1.46 oil DIC (UV) VIS-IR) and three lasers at wavelengths 488 nm (iBeam-Smart-CD), 642 nm (Coherent® Obis™ Galaxy Laser 1236445) and 532 nm (Oxxius L1C). A dichroic mirror (Di01-R405/488/532/635-25x36, Semrock) was used to separate the emission from the excitation spectra. The emission spectrum was again split into two channels by an Optosplit II image splitter (Oxford Instruments), which contained an additional dichroic mirror (DD640-FDi01-25x36, Semrock) as well as two emission filters (ET 570/60, ET 675/50, Chroma). The signal was recorded using an EMCCD camera (Andor iXon Ultra) (pixel size 16 μm^2) which was operated at a temperature of -60°C. The LabVIEW program *SDT-Control* was used to operate the setup. Laser type and percentage of power were chosen as well as the imaging parameters. Adjustments for the 532 nm laser were done in the software *Oxxius Lasers*(Oxxius SA). The TIRF angle could be adjusted with the LabVIEW program *Servotisch* and was chosen individually for each measurement set. Before placing the chamber onto the sample holder, the objective as well as the bottom of the LTC were cleaned with ethanol and a droplet of immersion oil (Carl Zeiss™ Immersol™ 518) was applied to the objective. All measurements were conducted

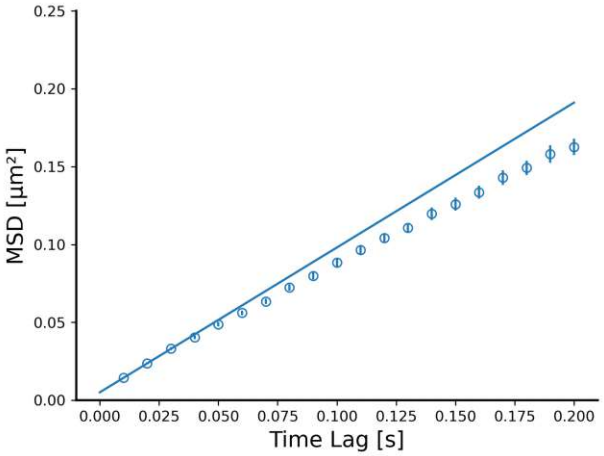

Figure 3.2.: ***Exemplary mean squared displacement (MSD) analysis for diffusive behavior of DNA origami platforms***. *MSDs across all trajectories are plotted over time lag t. The diffusion coefficient can subsequently be determined by fitting equation 3.1 to the first two data points of the plot.*

at room temperature.

3.2.1. Diffusion Measurements

Data for diffusion measurements was obtained by imaging ten different positions in each well. An illumination time of 3 ms and a frame rate of 100 fps were chosen. In each position around 200 frames were recorded. Data was analysed using an in-house python [64] script based on the sdt-python package by Lukas Schrangl [65] (provided by Anežka Májková). The diffusion was determined via mean squared displacement (MSD) analysis. MSDs were calculated as the average across all trajectories and plotted as a function of the time lag t. The diffusion coefficient D was then obtained by fitting the function

$$MSD = 4Dt + 4\sigma_{xy} \tag{3.1}$$

with $4\sigma_{xy}$ referring to the localization precision, to the first two data points of the plot.

3.2.2. Surface Density Measurements

The surface density was determined by imaging ten different positions within each well, with an illumination time of 3 ms and a frame rate of 100 fps. In each

position, approximately 100 frames were recorded. Determining surface density required data on both bulk intensity and single molecule intensity. Initially, bulk intensity was recorded at a lower laser power for approximately four frames. The laser power was then increased for about 50 frames to facilitate bleaching, before being reduced once more. This bleaching process allowed for the recording of single molecule signals. The data was analyzed using an in-house python script (provided by Anežka Májková).

To determine the surface density, first a region of interest (ROI), within which all signals have the same intensity, is chosen. The background corrected bulk intensity I_{CORR} within the ROI is then calculated by subtracting the background intensity I_{BACK} from the mean intensity I_{RAW}. With this corrected value, surface density ρ within the ROI is calculated by dividing the corrected intensity by the single molecule intensity I_{SMI} multiplied by the pixel size (Equation 3.2).

$$\rho \left[\frac{signals}{\mu m^2}\right] = \frac{I_{CORR}\left[\frac{counts}{px}\right]}{I_{SMI}\left[\frac{counts}{signal}\right] \cdot 0.16^2 \left[\frac{\mu m^2}{px}\right]} \tag{3.2}$$

3.2.3. Co-Localization Measurements

For the co-localization measurements, the sample was imaged in ten different positions in each well with an illumination time of 3 ms and a frame rate of 100 fps. One frame was recorded per position. The sample was imaged in two channels simultaneously, with one channel visualizing the platforms and the other visualizing the ligands. With the help of an in-house python script (provided by Anežka Májková), the percentage of overlay between the two channels, corresponding to the efficiency with which pMHC was bound to the DNA origami platforms, was measured (Fig. 3.3).

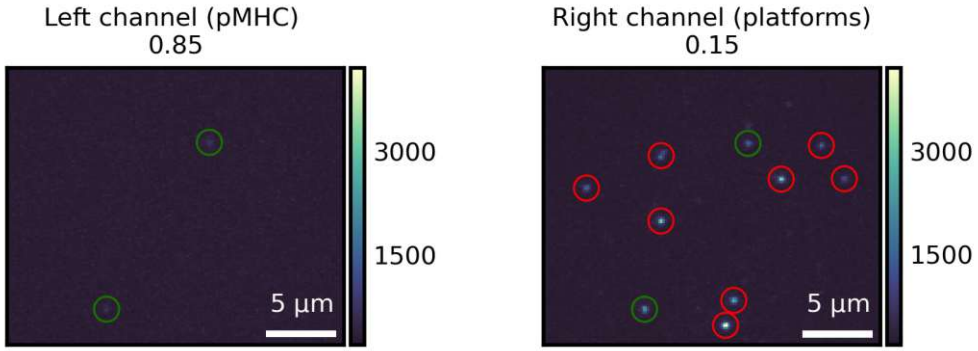

Figure 3.3.: ***Exemplary co-localization analysis of platform:pMHC binding.*** *Samples are imaged in two different color channels simultaneously. The brightness intensity is displayed in arbitrary units. Green circles indicate signals that have been localized in both channels, while red circles indicate the presence of a signal in only one of the two measuring channels. The given percentages of overlay correspond to the efficiency with which pMHC was bound to the DNA origami platforms.*

To calculate the overlay percentages the number of colocalized signals, N_{coloc}, was compared to the total number of signals. The fraction of DNA origami platforms that carry a pMHC ligand, f_1, was calculated by comparing N_{coloc} to the total number of platform signals, N_1 (see Equation 3.3). The fraction of pMHC ligands bound to a DNA origami platform, f_2, was determined by comparing N_{coloc} to the total number of ligand signals, N_2 (see Equation 3.4). Calculated fractions represent the mean of all ten imaged positions, figures displaying the colocalization only show exemplary positions.

$$f_1 = \frac{N_{coloc}}{N_1} \tag{3.3}$$

$$f_2 = \frac{N_{coloc}}{N_2} \tag{3.4}$$

4. Results

4.1. Thermal Folding of DNA Origami

The quality of three different thermal folding protocols ("1 min", "10 min", "60 min", see Table 4.1) was assessed via agarose gel electrophoresis. A folding protocol was deemed of "good quality" if there were no signs of aggregates visible in the gel and the results were consistently reproducible. The data was gathered over a period of three weeks, which included ten distinct days of experiments. Besides quality analysis via agarose gel electrophoresis, some samples were additionally analyzed via TIRF microscopy to image aggregates (Fig. 4.2). Furthermore, the yield of each method was compared, which was obtained by ultra-filtrating the folded samples and subsequently measuring their molar concentration and total mass. All experiments were conducted with one of two different DNA origami mixes (see Appendix A, Table A.1 and A.2), with the main difference being the presence of AF555. Errors were calculated as the standard error of the mean (sem) σ_x using the following formula: $\sigma_x = \frac{\sigma}{\sqrt{n}}$, where σ is the standard deviation and n is the number of observations.

For each sample an amount of 100 µL DNA origami solution was mixed. Considering the yields, all protocol variation performed similarly with a molar concentration and total mass of 6.9 ± 1.31 nM (mean ± sem) and 1,780 ± 445 ng (mean ± sem) for the "1 min" folding protocol, 7.2 ± 1.30 nM (mean ± sem) and 1,717 ± 430 ng (mean ± sem) for the "10 min" folding protocol and 6.9 ± 1.21 nM (mean ± sem) and 1,637 ± 418 ng (mean ± sem) for the "60 min" folding protocol (see Tab. 4.1).

The quality of folded DNA origami platforms was found to vary for all variations of tested thermal folding protocols. The formation of aggregates could not be attributed to a specific folding protocol, rather, it appeared to occur randomly (see Fig. 4.1). Although the quality of the folded DNA origami was found to be superior when folded using the "60 min" protocol, random outliers were observed for all protocols tested, introducing a level of uncertainty into the process. Another point to be considered was the time required for completion of each protocol. Even though the "60 min" protocol delivered promising results, its total runtime of two days rendered it unsuitable for routine utilization.

Consequently, a new thermal folding protocol, shown in Figure 4.3a, was

Table 4.1.: **Recovery yields from thermal folding protocols.** Each sample had an amount of 100 µL and was mixed from one of two mixing protocols. An "x" indicates the presence of AF555 in the DNA origami mix. For each protocol, the molar concentration and total mass yield per experiment day is shown, the overall mean and sem are included in bold.

Protocol	C_n [nM]	m_{total} [ng]	Fluorophore
1 min	4.8	1102.5	
	4.8	1283	x
	6.5	1617	
	6.5	1373	x
	11.9	3528	x
	6.9 ± 1.3	**1,780 ± 445**	
10 min	3.0	504	
	10.6	2900	x
	5.4	1160	x
	5.4	1148	x
	7.4	1470	
	11.1	3120	x
	7.2 ± 1.3	**1,717 ± 430**	
60 min	4.8	1305	x
	4.8	518	
	6.0	1344	
	11.3	3021	x
	7.4	1995	x
	6.9 ± 1.2	**1,637 ± 418**	
5 min	11.9	3472	x
	8.7	2035	x
	10.8	3293	x
	4.3	2140	x
	8.9 ± 1.7	**2,735 ± 376**	

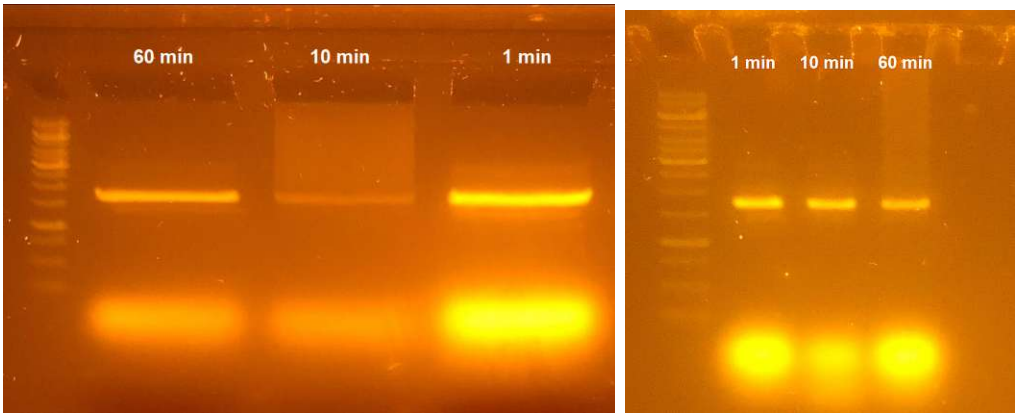

(a) (b)

Figure 4.1.: ***Quality of folding protocols on two distinct measurements days.*** *Agarose gel electrophoresis was carried out on ice at 65 V for 90 min.* ***(a)****. Samples folded with "1 min" and "10 min" folding protocols show the presence of aggregates, evident as additional bands above the main band containing correctly the folded DNA origami platforms.* ***(b)*** *"60 min" shows the presences of aggregates, while both "1 min" and "10 min" folding protocols have no visible aggregates. The presence of aggregates could not be attributed to one specific protocol, but rather appeared to be random.*

developed, combining the benefits of its predecessors, trying to create a reliable folding protocol that was as time efficient as possible. The sample is heated up to 90°C to ensure a complete denaturation of the components. To prevent potential damage to the sample due to thermal fluctuations as well as unspecific binding, it is cooled down again rapidly to 75°C. This temperature is held for 15 min to, again, ensure that all components are completely denatured. As the critical annealing process takes place between 75°C and 25°C, the cooling pace is slowed down to 1°C/5min in this temperature span. After reaching 25°C the annealing process is completed and the sample is rapidly cooled down to 4°C at which temperature it is held until further processing. The yields for this protocol (Tab. 4.1) were higher than those previously tested, with a molar concentration of 8.9 ± 1.67 nM (mean ± sem) and a total mass of 2,735 ± 376 ng (mean ± sem), which is likely not due to the protocol itself, but rather due to the use of newly ordered DNA origami strands. Figure 4.3b, also shows the presence of aggregates in the "5 min" folding protocol, however, these aggregates can be also seen in column two, displaying only the scaffold strands.

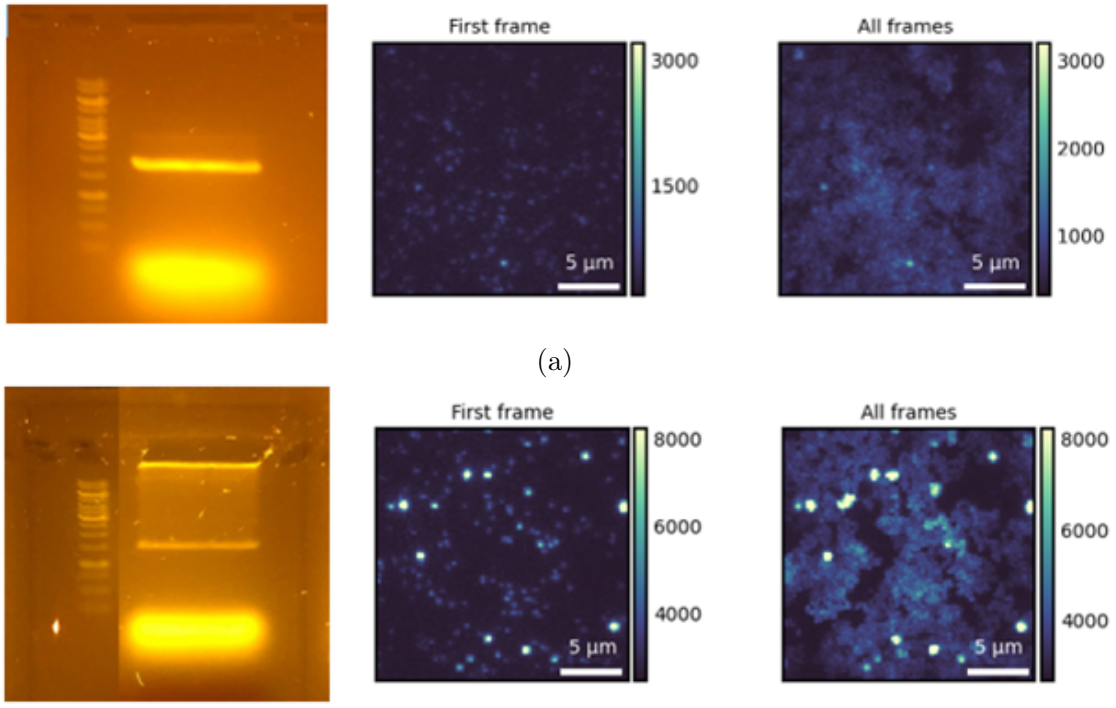

Figure 4.2.: ***Comparison between highly aggregated DNA origami sample (b) and sample with few aggregates present (a).*** *Results from agarose gel electrophoresis and TIRF diffusion experiments are shown. "First frame" represent the first image taken during diffusion measurement. Each signal corresponds to an DNA origami platform labeled with six AF555 fluorophores. "All frames" is a composition image summing up all images recorded during measurement. A blurry appearance indicates mobile platforms, while distinct bright signals indicate immobile platforms. The brightness intensity is displayed in arbitrary units. The comparison highlights the mobility differences between the two samples, where the sample displaying aggregations in gel results in more immobile platforms in TIRF diffusion experiments.*

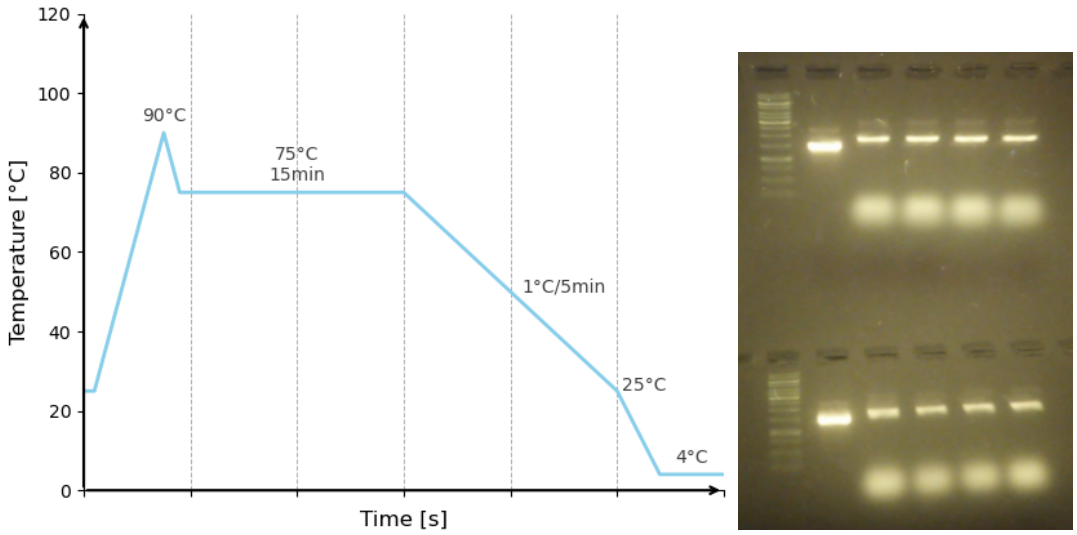

(a) (b)

Figure 4.3.: ***"5 min" thermal folding protocol.*** ***(a)*** *The presented plot illustrates an adjusted thermal protocol, which is designed to deliver the most stable results in the shortest possible time.* ***(b)*** *Agarose gel electrophoresis analyzing quality of "5 min" thermal folding protocol. Agarose gel electrophoresis was carried out on ice at 65 V for 90 min. Samples were folded in one thermocycler run, each in a different PCR tube. Column one and two show DNA ladder and scaffold, columns three to six show the samples.*

While the "60 min" folding protocol produced good quality results, its extensive runtime and occasional variability in quality made it unsuitable for routine utilization. In terms of yield, all three protocols performed equally well. As a result a new thermal folding protocol was developed to combine the relatively reliable results of the "60 min" protocol with the time efficiency of the other two. The developed protocol showed higher yields than its predecessors and was found to be reliable in routine use. Representative images and quantitative data are provided in Figure 4.1 - 4.3 as well as Table 4.1.

4.2. Purification Methods

The effectiveness of two different methods (ultra-filtration and agarose gel electrophoresis) for purifying DNA origami platforms was evaluated using diffusion measurements conducted over five distinct experimental days. All samples were prepared using the same mixing protocol (see Appendix A, Table A.1) and labeled with AF555. Except for the last experiment, for which the Freeze 'N Squeeze™ DNA Gel Extraction Spin Columns were used, all platforms purified by agarose gel electrophoresis were extracted manually from the gel. SLB functionalization was done without the addition of $MgCl_2$ in all experiments.

On the first experimental day, both the "10 min" and "60 min" folding protocols were used, each on 100 µL of DNA origami solution. Each sample was divided into two equal 50 µL portions, one for purification via ultra-filtration and the other by agarose gel electrophoresis. After purification, the ultra-filtrated samples from the "10 min" folding protocol had a molarity of 10.64 nM and a total mass of 2,900 ng. For the "60 min" folding protocol a molarity of 7.45 nM and a total mass of 1995 ng were measured. In contrast, samples purified via agarose gel electrophoresis yielded a molarity of 1.60 nM with a total mass of 390 ng for the "10 min" protocol, and 1.06 nM and of 170 ng for the "60 min" protocol. Diffusion measurements were performed using two wells, each containing 50 ng of DNA origami platforms per condition and folding protocol. For ultra-filtration diffusion values of 0.26 ± 0.02 $\mu m^2/s$ (mean ± sem) ("10 min") and 0.24 ± 0.01 $\mu m^2/s$ (mean ± sem) ("60 min") were measured, while gel electrophoresis produced diffusion values of 0.26 ± 0.02 $\mu m^2/s$ (mean ± sem) ("10 min") and 0.31 ± 0.01 $\mu m^2/s$ (mean ± sem) ("60 min").

For the second, third and fourth experimental days a consistent stock of 300 µL DNA origami platforms was utilized, which had previously been folded using the "10 min" folding protocol and was stored at -20°C. For each experimental day, 100 µL of stored DNA origami solution was divided into two 50 µL parts for purification. Ultra-filtration purified samples had molarities of 5.43 nM, 5.48 nM and 3.29 nM, with total masses of 1,161 ng, 1,288 ng and 649 ng, respectively. Agarose gel-purified samples had molar concentrations of 1.38 nM, 1.54 nM and 1.49 nM, with total masses of 897 ng, 1,791 ng and 994 ng, respectively. On the second and third days, diffusion measurements were performed using 50 ng of DNA origami platforms per well. On the fourth day of experiment, two wells containing 50 ng and two wells containing 20 ng of sample per condition were prepared. The measured diffusion values were 0.26 ± 0.02 $\mu m^2/s$ (mean ± sem) for ultra-filtration and 0.27 ± 0.03 $\mu m^2/s$ (mean ± sem) for gel electrophoresis on the second experimental day, 0.30 ± 0.00 $\mu m^2/s$ (mean ± sem) for ultra-filtration and 0.28 ± 0.01 $\mu m^2/s$ (mean ± sem) for gel electrophoresis on the third experimental day and 0.24 ± 0.01 $\mu m^2/s$ (mean ± sem) for ultra-filtration and 0.21 ± 0.01 $\mu m^2/s$ (mean ± sem) for gel electrophoresis on the fourth experimental day.

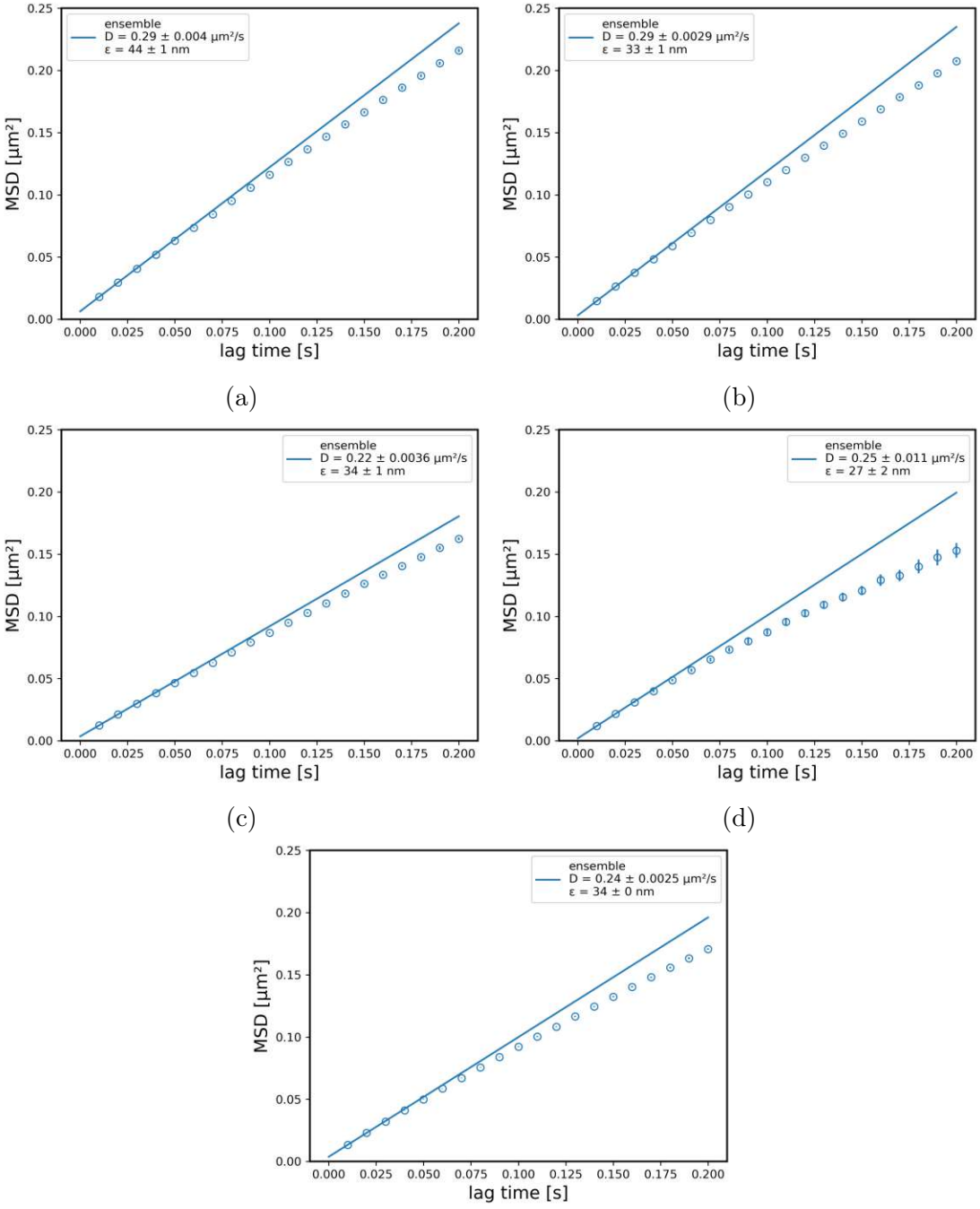

Figure 4.4.: ***MSD Analysis of DNA origami platforms purified via agarose gel electrophoresis.*** *Measurements were conducted on five separate occasions, exemplary images per experimental day are shown. An average diffusion of 0.261 ± 0.01 µm²/s was calculated.*

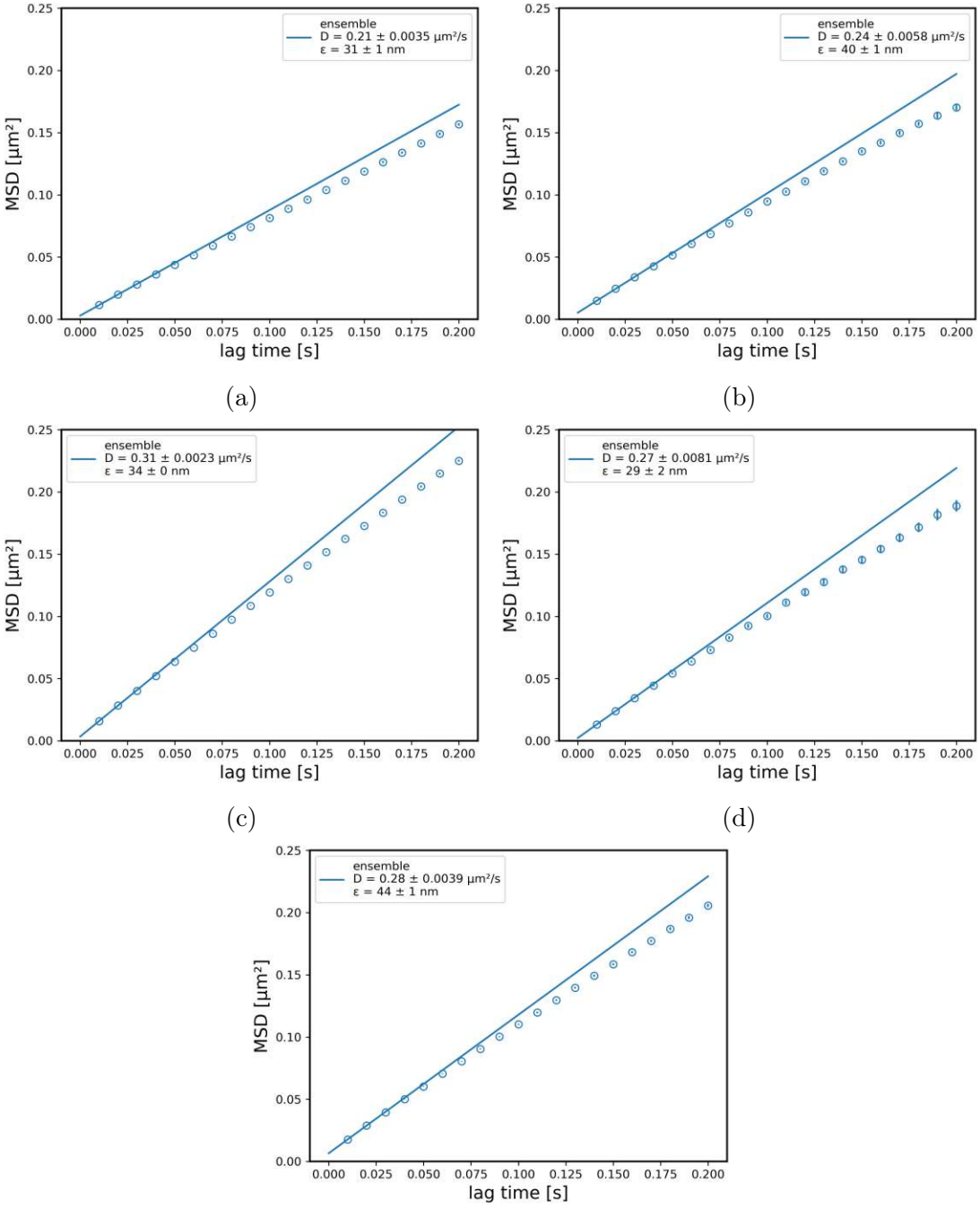

Figure 4.5.: ***MSD Analysis of DNA origami platforms purified via ultrafiltation.*** *Measurements were conducted on five separate occasions, exemplary images per experimental day are shown. An average diffusion of 0.261 ± 0.01 $\mu m^2/s$ was calculated.*

Table 4.2.: **Molar concentration and total masses of purified DNA origami platforms.** All DNA origami solutions were mixed according to the same mixing protocol (Tab. A.1). Each purification was performed on 50 µL unpurified DNA origami solution. The mean and sem are included in bold.

	Ultra-filtration			Agarose gel electrophoresis		
Protocol	C_n [nM]	m_{total} [ng]	D [µm^2/s]	C_n [nM]	m_{total} [ng]	D [µm^2/s]
10 min	10.64	2,900	0.26 ± 0.02	1.60	390	0.26 ± 0.02
60 min	7.45	1,995	0.24 ± 0.01	1.06	170	0.31 ± 0.01
10 min	5.43	1,161	0.26 ± 0.02	1.38	897	0.27 ± 0.03
10 min	5.48	1,288	0.30 ± 0.00	1.54	1,791	0.28 ± 0.01
10 min	3.29	649	0.24 ± 0.01	1.49	994	0.21 ± 0.01
5 min	13.19	2,480	0.27 ± 0.01	1.70	3,040	0.23 ± 0.03
	7.58 ± 1.5	**1,745 ± 351**	**0.26 ± 0.01**	**1.46 ± 0.09**	**1,213 ± 431**	**0.26 ± 0.01**

On the final experimental day, 100 µL of DNA origami platforms were folded with the "5 min" folding protocol and evenly divided between purification methods. Platforms purified via ultrafiltration had a molarity of 13.19 nM and a total mass of 2,480 ng, while agarose gel electrophoresis purified platforms had a molar concentration of 1.7 nM with a total mass of 3,040 ng. Diffusion measurements for agarose gel-purified samples included two wells containing 470 ng and 70 ng, while ultra-filtration samples were measured in three wells containing 750 ng, 300 ng, and 70 ng. For ultra-filtration a diffusion of 0.27 ± 0.01 µm^2/s (mean ± sem), while gel electrophoresis produced a diffusion of 0.23 ± 0.03 µm^2/s (mean ± sem).

Figure 4.4 and 4.5 illustrate the exemplary MSD analysis of agarose gel-purified and ultra-filtration purified samples, respectively. Each figure depicts a measurement from one well obtained on a distinct day. Across all experimental days, the calculated mean diffusion values were identical for both methods, at 0.26 ± 0.01 µm^2/s (mean ± sem). No visible aggregates were present in any of the imaged samples.

The measured concentrations, yields and diffusion values are summarized in Table 4.2. Ultra-filtration consistently produced higher molar concentration values (7.58 ± 1.50 nM (mean ± sem)) than gel-purification (1.46 ± 0.1 nM (mean ± sem)). The total mass yield for ultra-filtration, with an average of 1,745 ± 351 ng (mean ± sem) was comparable to the results for agarose gel purified samples with an average of 1,217 ± 432 ng (mean ± sem).

Although the choice of purification method did not affect the diffusion properties of the DNA origami platforms, and both methods achieved comparable yields, ultra-filtration was advantageous in this application, as it was significantly less time-consuming and labor-intensive. These findings highlight ultra-filtration as the preferred method for purifying DNA origami platforms in studies, that require efficient preparation, while gel purification should be used in applications, in which the quality (i.e. "non-aggregated") of DNA origami structures is paramount.

4.3. DNA Origami Functionalization

The experiment was conducted over three independent days, with details of the mixing protocol provided in Appendix A, Table A.3. Platforms were prepared using AF488, and biotinylated pMHC was labeled with Alexa Fluor™ 647 (AF647). Three protocol variations (functionalization with mSA one day in advance, complete functionalization on the day of the experiment and complete functionalization on the day of the experiment without any purification steps in between) were tested to examine the influence of preparation time on the efficiency of platform:pMHC binding.

The efficiency of pMHC binding to DNA origami platforms was evaluated using co-localization measurements. Samples were imaged simultaneously in two channels. The left channel captured the signal from pMHC, while the right channel captured the signal from the DNA origami platforms. Overlay percentages for each channel were calculated based on the alignment of signals in order to assess the binding efficiency of pMHC to the DNA origami platforms (see Equations 3.3 and 3.4).

For the first experiment, three variations of the functionalization protocol were tested. 100 µL DNA origami solution was prepared using the "5 min" folding protocol, and SLB functionalization was performed with the addition of $MgCl_2$, samples were purified via ultra-filtration. Purified platforms had a molar concentration of 11.9 nM with a total mass of 3,472 ng. For variations one and two, 10 µL (347 ng) of purified DNA origami solution each were incubated with mSA at room temperature, followed by purification. Variation one resulted in platforms with a molar concentration of 0.64 nM and a total mass of 156 ng, while variation two produced a molar concentration of 0.74 nM with a total mass of 150.5 ng. For variation three, 10 µL of platform solution was mixed directly with mSA and pMHC without a purification step. For each variation, two wells containing 10 ng and two wells containing 1 ng of functionalized platform solution were prepared, measurements were conducted exclusively on the 10 ng wells.

Table 4.3.: **Yields and overlay percentages of three different DNA origami functionalization protocols.** f_1 denotes the fraction of DNA origami platfroms carrying a pMHC, f_2 denotes the fraction of pMHC that is bound to a DNA origami platfrom. Variation one was prepared over a period of two days, while protocol variation two was prepared over one day. For protocol variation three, sample incubation with mSA and pMHC were done at once, omitting the purification step in between. f_1 and f_2 are given as mean ± sem.

Variation	C_n [nM]	m_{total} [ng]	f_1	f_2
1	0.64	156	0.15 ± 0.01	0.85 ± 0.06
2	0.74	150.5	0.24 ± 0.02	0.83 ± 0.01
3	11.9	347	0.07 ± 0.03	0.82 ± 0.08

The results of the first experiment (see Tab. 4.3) showed distinct differences in overlay percentages among the protocol variations. For variation one, mean overlay percentages of 0.85 ± 0.06 (pMHC) and 0.15 ± 0.01 (platforms) were observed. Variation two yielded similar results for pMHC, with a mean overlay percentage of 0.83 ± 0.01, but showed improved efficiency for the platforms with 0.24 ± 0.02. In contrast, variation three resulted in the lowest overlay percentages, with 0.82 ± 0.08 (pMHC) and 0.07 ± 0.03 (platforms). Co-localization measurements for each variation are depicted in Fig. 4.6. Given the significantly lower efficiency of variation three, it was excluded from subsequent experiments.

For the second and third experiment, the potential influence of mSA-incubation temperature on platform:pMHC binding was investigated in addition to the influence of preparation time. 300 µL of DNA origami solution was prepared using the "5 min" folding protocol, and SLB functionalization was performed using the $MgCl_2$ mediated method. Ultra-filtration purified platforms had a molar concentration of 32 nM and a total mass of 9,880 ng. Per condition, 5 µL (490 ng) of purified platform solution was used. The measured molarities and total masses can be found in Table 4.4. For the second experiment, two wells per condition were prepared, each containing 10 ng of DNA origami platforms. For the third experiment, one well contained 10 ng, and another contained 1 ng of DNA origami platforms for each condition.

The results from these experiments (Tab. 4.4) revealed no significant difference in overlay percentages between mSA-incubation at room temperature and at 37°C (Fig. 4.9b). For room temperature incubation, overlay percentages were 0.92 ± 0.01 for the left channel (pMHC) and 0.25 ± 0.03 for the right channel (DNA origami platforms). At 37°C, the overlay percentages were 0.83 ± 0.08 for pMHC

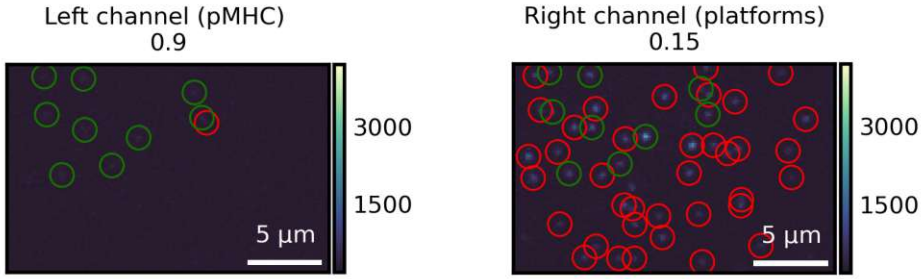

(a)

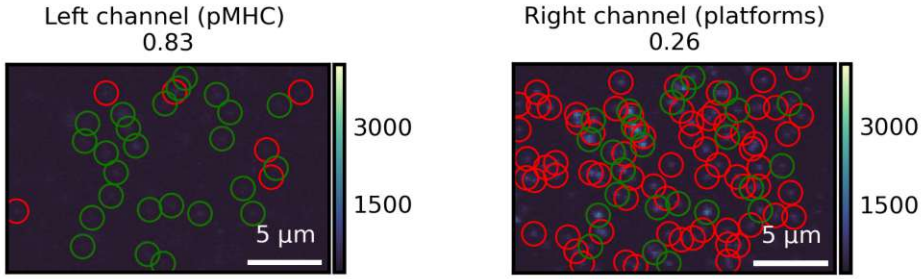

(b)

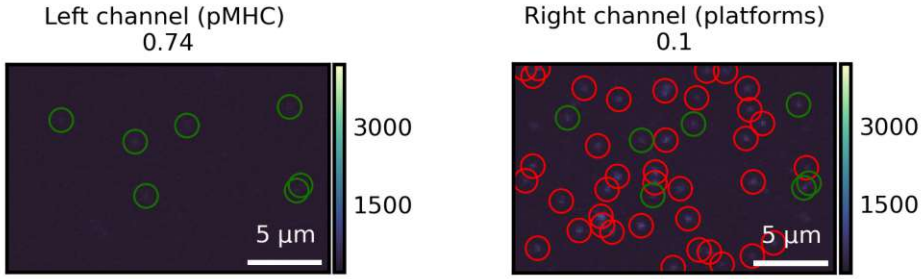

(c)

Figure 4.6.: ***Co-localization measurements investigating the influence of preparation time on platform:pMHC binding efficiency.*** *AF647 labeled pMHC was imaged in the red channel (left), platforms were labeled with six AF488 fluorophores and imaged in the blue channel (right). SLBs were incubated with 10 ng of functionalized DNA origami platforms. The brightness intensity is displayed in arbitrary units. Measurements are taken from experiment one. Depicted are distinct measurements in one well from each protocol variation, the overall mean and sem were calculated from all measurements of each protocol variation (a minimum of two wells).* ***(a)*** *For protocol variation one, mean overlay percentages of* $f_1 = 0.15 \pm 0.01$ *(platforms) and* $f_2 = 0.85 \pm 0.06$ *(pMHC) were observed.* ***(b)*** *For variation two, mean overlay percentages of* $f_1 = 0.24 \pm 0.02$ *(platforms) and* $f_2 = 0.83 \pm 0.01$ *(pMHC) were observed.* ***(c)*** *For variation three, mean overlay percentages of* $f_1 = 0.07 \pm 0.03$ *(platforms) and* $f_2 = 0.82 \pm 0.08$ *(pMHC) were observed.*

Table 4.4.: **Molarity and total mass of ultra-filtration purified functionalized DNA origami platforms.** f_1 denotes the fraction of DNA origami platfroms carrying a pMHC, f_2 denotes the fraction of pMHC that is bound to a DNA origami platfrom. Two different preparation variations were compared. Variation one was prepared over a period of two days, while variation two was prepared over a period of one day.

Protocol		C_n [nM]	m_{total} [ng]	f_1	f_2
1	RT	0.74	228	0.19 ± 0.02	0.94 ± 0.00
		0.85	264	0.18 ± 0.03	0.94 ± 0.04
	37°C	0.96	276	0.19 ± 0.01	0.92 ± 0.01
		0.74	300	0.14 ± 0.02	0.56 ± 0.30
		0.82 ± 0.05	**267 ± 15**	**0.17 ± 0.01**	**0.84 ± 0.08**
2	RT	0.90	276	0.32 ± 0.01	0.91 ± 0.01
		1.06	300	0.32 ± 0.02	0.90 ± 0.03
	37°C	0.64	195	0.33 ± 0.02	0.9 ± 0.01
		1.15	324	0.36 ± 0.04	0.96 ± 0.00
		0.94 ± 0.11	**274 ± 28**	**0.33 ± 0.01**	**0.92 ± 0.01**

and 0.25 ± 0.04 for the platforms.

For preparation times, on the other hand, a clear improvement in platform:pMHC binding efficiency was observed for protocol variation two, in which DNA origami functionalization was carried out completely on the day of measurement (Fig. 4.9a). This variation achieved overlay percentages of 0.90 ± 0.02 for pMHC and 0.31 ± 0.01 for platforms. Variation one, which involved preparation over two days, resulted in lower overlay percentages of 0.84 ± 0.07 for pMHC and 0.17 ± 0.01 for platforms.

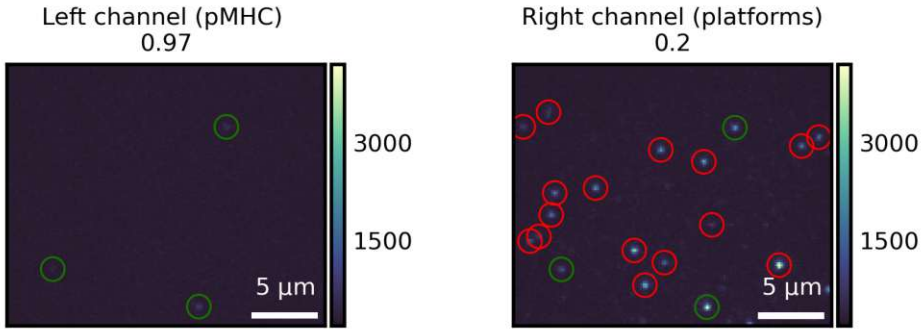

(a)

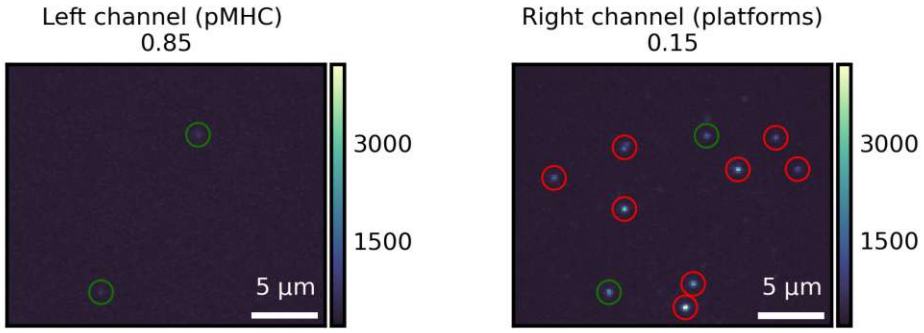

(b)

Figure 4.7.: ***Co-localization measurements of functionalization protocol variation one.*** *DNA origami platform functionalization was performed over two consecutive days. AF647 labeled pMHC was imaged in the red channel, platforms were labeled with six AF488 fluorophores and imaged in the blue channel. SLBs were incubated with 1 ng of functionalized DNA origami platforms. The brightness intensity is displayed in arbitrary units. Depicted are two distinct measurements in one well per condition, overall mean and sem were calculated from data gathered from experiments two and three (two independent experiments, per each a minimum of two wells were measured).* ***(a)*** *Platform incubation with mSA at RT. Overlay percentages of* $f_1 = 0.18 \pm 0.01$ *(platforms) and* $f_2 = 0.94 \pm 0.01$ *(pMHC) were observed.* ***(b)*** *Platform incubation with mSA at 37°C. Overlay percentages of* $f_1 = 0.16 \pm 0.02$ *(platforms) and* $f_2 = 0.74 \pm 0.02$ *(pMHC) were observed.*

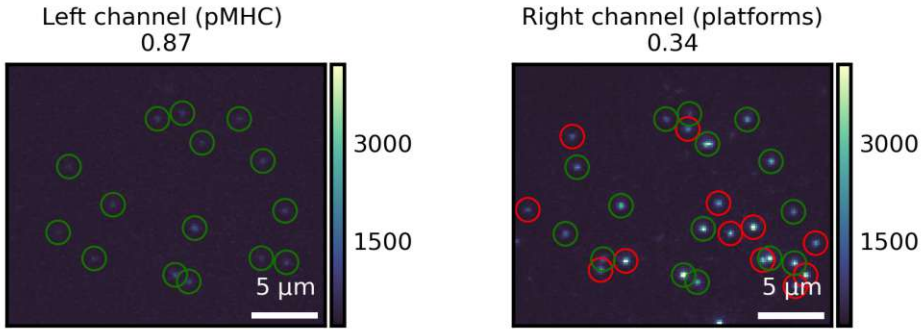

(a)

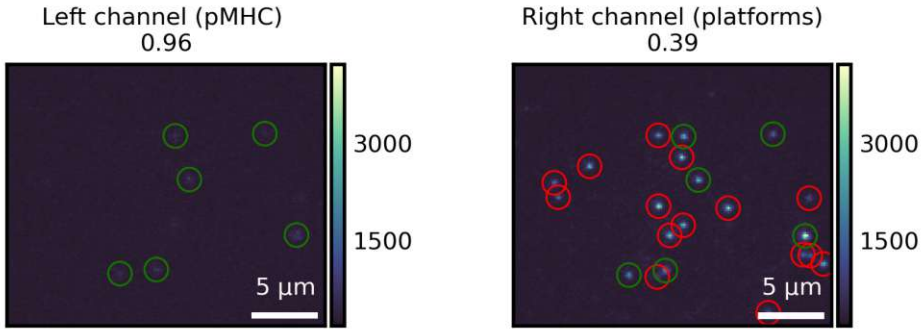

(b)

Figure 4.8.: ***Co-localization measurements of functionalization protocol variation two.*** *DNA origami platform functionalization was performed on one day. AF647 labeled pMHC was imaged in the red channel, platforms were labeled with six AF488 fluorophores and imaged in the blue channel. SLBs were incubated with 1 ng of functionalized DNA origami platforms. The brightness intensity is displayed in arbitrary units. Depicted are two distinct measurements in one well per condition, overall mean and sem were calculated from data gathered from experiments two and three (two independent experiments, per each a minimum of two wells were measured).* ***(a)*** *Platform incubation with mSA at RT. Overlay percentages of* $f_1 = 0.32 \pm 0.01$ *(platforms) and* $f_2 = 0.90 \pm 0.01$ *(pMHC) were observed.* ***(b)*** *Platform incubation with mSA at 37°C. Overlay percentages of* $f_1 = 0.34 \pm 0.02$ *(platforms) and* $f_2 = 0.93 \pm 0.02$ *(pMHC) were observed.*

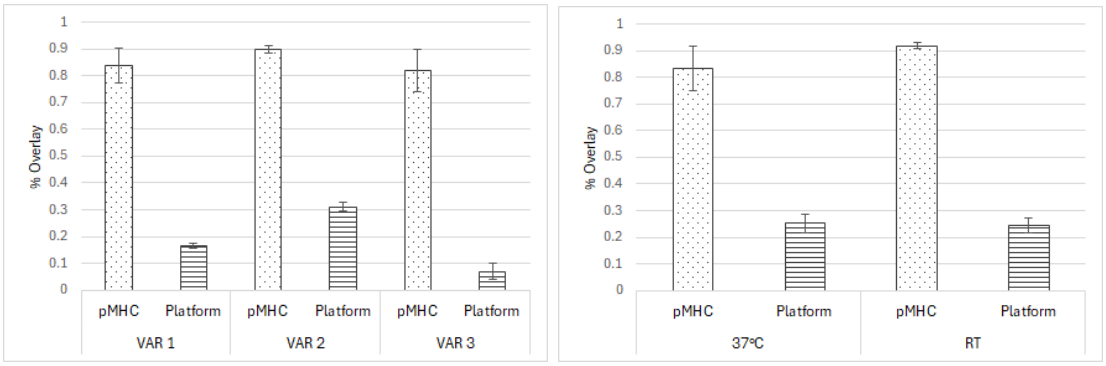

(a) (b)

Figure 4.9.: ***Co-localization measurements investigating the influence of preparation time and incubation temperature on platform:pMHC binding efficiency.*** *Error bars were derived as the sem.* ***(a)*** *Comparison between protocol variations. The mean was calculated over all available measurements. Variation two shows a higher percentage of overlay between pMHC and platforms, compared to the other two protocol variations.* ***(b)*** *Comparison between mSA-incubation temperature. The means were calculated from the data gathered from experiments two and three. No apparent difference can be observed between the two conditions.*

The findings clearly indicate that functionalization of DNA origami platforms on the days of measurement, as demonstrated in protocol variation two, significantly enhances platform:pMHC binding efficiency. This protocol consistently achieved higher overlay percentages. Incubation temperature on the contrary, had no influence on binding efficiency, as depicted in Figure 4.9b. Representative co-localization images and quantitative data are provided in Figures 4.6 - 4.9, illustrating the improvements achieved through optimized protocols.

4.4. SLB Functionalization

Surface density measurements were conducted on two separate days in order to assess the efficiency of two distinct methods (functionalization without $MgCl_2$ and functionalization with $MgCl_2$) for binding DNA origami platforms to SLBs. All experiments were carried out using the same stock solution of purified DNA origami platforms, labeled with six AF488 fluorophores and one abberior STAR 635P (AS635P), which was prepared following the mixing protocol provided in Appendix A, Table A.4. 100 µL of DNA origami solution was prepared using the "1 min" thermal folding protocol, and folded platforms were subsequently purified via ultra-filtration. The resulting solution had a molarity of 77 nM and contained a total mass of 27,874 ng of DNA origami platforms. On both experimental days platforms were measured in the red channel, imaging AS635P only.

Table 4.5.: **Surface densities of two different SLB functionalization approaches.** The approach with the addition of $MgCl_2$ yielded surface densities that were about fivefold (20 ng) and tenfold (100 ng) higher than those obtained without $MgCl_2$. Mean and sem are included in bold.

	Surface density [µm^{-2}]	
DNA origami	without $MgCl_2$	with $MgCl_2$
20 ng	0.12	0.54
	0.10	1.00
	0.14	0.69
	0.15	0.82
	0.13 ± 0.01	**0.76 ± 0.10**
100 ng	0.69	5.47
	0.51	6.55
	0.55	4.98
	0.58	4.63
	0.58 ± 0.04	**5.41 ± 0.42**

In the first experiment, four wells containing 20 ng of DNA origami platforms each were prepared per condition. Functionalization without $MgCl_2$ yielded a surface density of 0.13 ± 0.01 µm^{-2} (mean ± sem) in comparison to 0.76 ± 0.10 µm^{-2} (mean ± sem) for functionalization with $MgCl_2$. This translates to a fivefold increase in surface density. On the second experimental day, each well was prepared with 100 ng of DNA origami platforms. Figure 4.10 illustrates two distinct

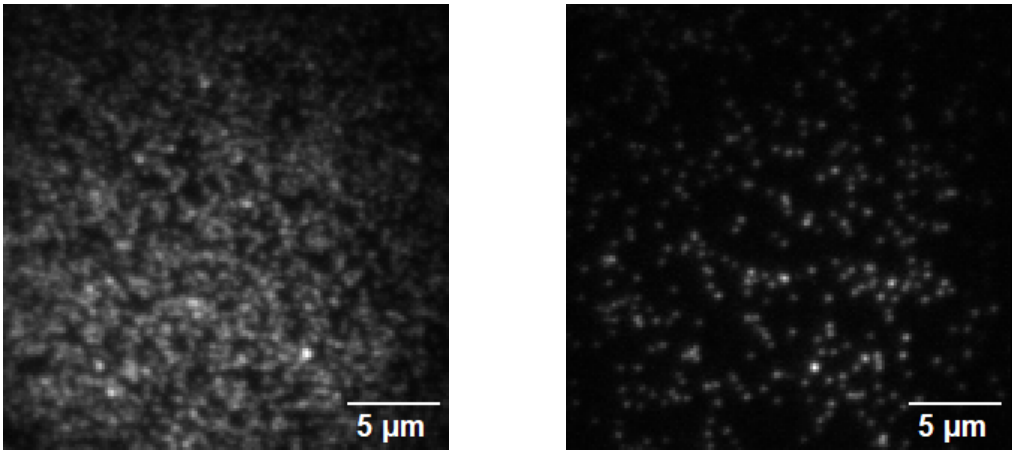

(a) (b)

Figure 4.10.: ***Comparison of bulk brightness between SLB functionalization (a)*** *with $MgCl_2$ and* ***(b)*** *without $MgCl_2$. Both samples were prepared with 100ng of DNA origami platforms. Images were conducted via TIRF microscopy.*

bilayers from the second experimental day as observed through TIRF microscopy. Figure 4.10a was functionalized with $MgCl_2$, whereas Figure 4.10b displays functionalization without $MgCl_2$. Functionalization without $MgCl_2$ yielded a surface density of 0.58 ± 0.04 μm^{-2} (mean $\pm$ sem), whereas functionalization with $MgCl_2$ delivered a surface density of 5.4 ± 0.42 μm^{-2} (mean $\pm$ sem), indicating a tenfold yield for the latter approach (see Fig. 4.11). In terms of the time required for preparation, both methods were found to be approximately equivalent.

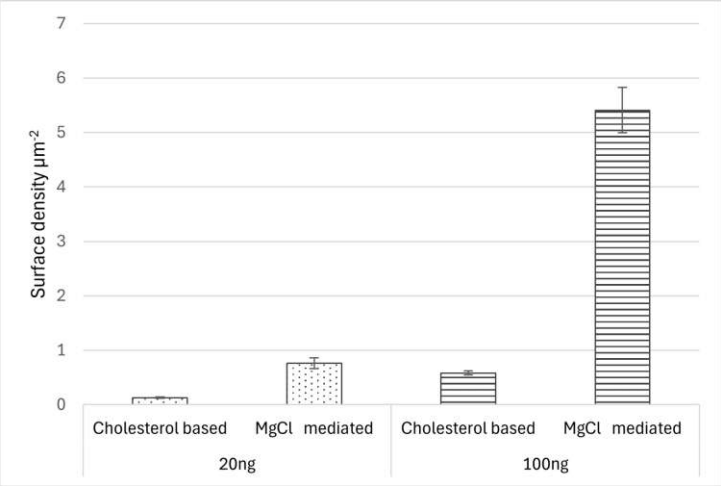

Figure 4.11.: ***Calculated average surface density between SLBs functionalized with versus without the addition of $MgCl_2$.*** *Functionalization with $MgCl_2$ showed higher platform densities for both 20 ng and 100 ng of DNA origami platfroms.*

The findings indicate, that the functionalization of SLBs with the addition of $MgCl_2$, enhances platform:SLB binding efficiency, as this protocol consistently achieved higher surface densities compared to an approach using soley cholesterol-DNA. These findings are also in accordance with the binding behavior observed during routine laboratory work. Quantitative data emphasizing these results can be found in Table 4.5 and Figure 4.11.

5. Discussion

5.1. Thermal Folding of DNA Origami

The thermal folding of DNA origami typically involves two key steps. First, the sample is heated, so any aggregated or entangled DNA is broken apart, before the sample is slowly cooled, during which the DNA origami can fold into the desired structures.

The hypothesis for these experiments was, that longer folding times would equal higher percentage of correctly folded origami. This assumption was expected to be reflected in the results of the gel purification as well as the overall yield. However, this was not supported by the findings. None of the tested protocols was superior compared to the others. Although the "60 min" protocol had a tendency for less visible aggregates in the gel, random outliers appeared across all folding protocols, and the yields remained consistent regardless of protocol used (Tab. 4.1).

Given the lack of consistent control over the folding process, a new protocol was developed to maximize the limited control available. The newly created protocol begins by heating the sample to 90°C, as in the "1 min" protocol, to ensure complete denaturation of the sample. Instead of maintaining this high temperature for an extended period, which could risk heat damage to the strands, the sample is cooled to 75°C and held there for 15 minutes. The stepwise cooling rate of 1°C/5 min was chosen to give the sample enough time to properly fold while keeping the runtime of the folding protocol within limits. The yields of the newly created protocol (Tab. 4.1) suggest a significant improvement in efficacy. However, this improvement is likely to be attributed to the use of newly ordered strands, rather than the protocol itself, as the strands used for comparing "1 min", "10 min" and "60 min" folding protocols were ordered in 2018, even though the shelf life of staple strands, as recommended by the manufacturer, is a maximum of two years. This hypothesis could be tested in a future experiment, by comparing yield and diffusion of the old and new strands.

Literature suggests, that the complexity of DNA origami structures, highly influence the required folding time. For simple 2D structures a folding time of as little as two hours has been reported [63], while 3D structures may require folding times of up to a week [43]. Intermediate folding times have also been employed [31, 46, 66]. Douglas et al. [43] have proposed, that the quality of folded DNA

origami structures can be improved by adjusting the cation concentration in the folding buffer. Their findings suggest, that insufficient cation concentrations can inhibit proper folding, while excessive concentrations can lead to the aggregation of the sample. In their work, a $MgCl_2$ concentration of 16 mM was chosen, while in other papers $MgCl_2$ concentrations between 6 mM and 16 mM have been commonly employed [31, 46, 63, 66]. The folding experiments conducted for this thesis were carried out with $MgCl_2$ concentrations of 10 mM and 12.5 mM.

In case of ongoing issues with aggregation, it is advised that cation concentration levels are adjusted. Otherwise, the folding time should be chosen according to the complexity of the structure. There is no need to prolong the folding times of simple DNA origami structures, as the quality of folded DNA origami cannot be reliably improved. The folding protocol created in this project delivers results, that are as reliable as can be and is recommended for use with simple 2D DNA origami structures.

5.2. Purification Methods

The results of the purification experiments indicate, that purification via ultra-filtration is the preferred method to agarose gel electrophoresis for the application in T-cell activation measurements. Both methods achieved the same overall diffusion value of 0.26 ± 0.01 $\mu m^2/s$ (mean $\pm$ sem), however ultra-filtration proved to be considerably easier to implement into routine work, being both more time-efficient and less labor-intensive. Despite these advantages, several points still have to be considered.

One important consideration is, that while ultra-filtration purified samples exhibited little to no aggregation during the course of these experiments, this is not always guaranteed. As established in the investigation of thermal folding protocols, proper folding is not always consistent and aggregates can form randomly, making them virtually impossible to fully prevent. As shown in Figure 5.1, there is always a possibility of an immobile fraction of aggregates, that can lower the sample's diffusion value.

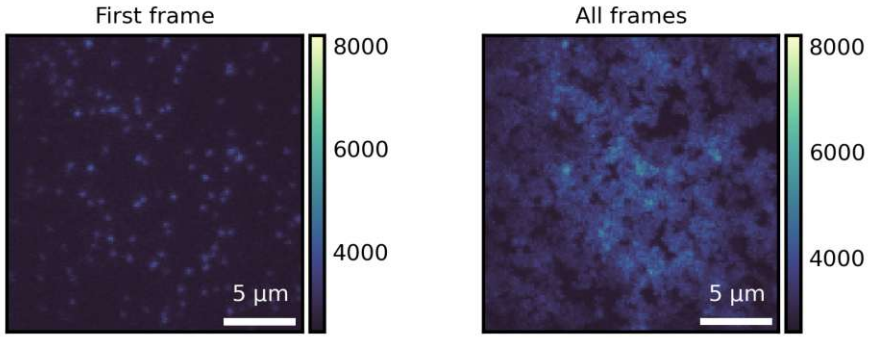

(a)

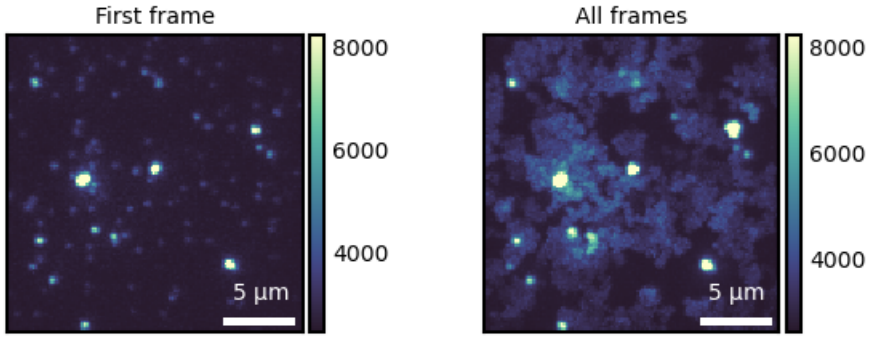

(b)

Figure 5.1.: ***Comparison between (a) gel-purified DNA origami samples and (b) samples purified via ultra-filtration.*** *"First frame" represent the first image taken during measurement. Each signal corresponds to an DNA origami platform labeled with six AF555 fluorophores. "All frames" is a composition image summing up all images recorded during TIRF measurement. A blurry appearance indicates mobile platforms, while distinct bright signals indicate immobile platforms. The brightness intensity is displayed in arbitrary units. Both measurements were done on the same experiment day, unpurified DNA origami platforms came from the same stock solution. For* ***(a)*** *a diffusion value of 0.32 ± 0.00 µm²/s was calculated, while for* ***(b)*** *the calculated diffusion value was 0.23 ± 0.00 µm²/s. The lower diffusion originates from the presence of an immobile fraction of aggregates in* ***(b)****, that cannot be filtered out with ultra-filtration.*

A possible workaround for this problem is establishing quality control of DNA origami after folding. Running a small quantity of sample an agarose gel can help visualize potential aggregation. However, since this adds an additional laborious step, DNA origami could be folded in larger batches and stored for extended use, as purified platforms can be stored up to four weeks at -20°C [1].

One of the main advantages of agarose gel purification is its ability to consistently yield high-quality DNA origami structures, regardless of variations in quality after folding. This is particularly crucial for applications requiring high quality structures. However, in the case of DNA origami platforms used in these experiments, the structures are relatively simple and therefore have a lower likelihood of misfolding. Additionally, the potential impact of SYBR™ Safe DNA Gel Stain, needed in the process of agarose gel electrophoresis, on T-cell activation has yet to be assessed.

5.3. DNA Origami Functionalization

The findings clearly indicate, that platform functionalization on the day of the experiment significantly improves the percentage of DNA origami platforms with pMHC bound. There are several possible explanations for this observation.

Binding stability between the oligonucleotide-modified streptavidin (mSA) and the complementary platform extension could have been insufficient, leading to bond breakage during the time between functionalization and actual usage. To test this assumption estimations from Taylor et al. [44] were utilized. Taylor et al. calculated the half-lives of various DNA sequences binding to their complementary strands. They found that the longer the investigated sequence, the longer the corresponding half-life of the bond. Besides experimentally determining the half-lives, Taylor et al. also calculated off-rates using computational analysis with the software *NUPACK* [67], which estimates Gibbs free energy of a DNA structure under specific conditions. At 37°C they determined a half-life of ∼24 s (ΔG = -12.16 kcal/mol) for a 13-mer sequence , while a 16-mer sequence was predicted to have a half-life of $>$ 7 hours (ΔG = -15.85 kcal/mol). In this thesis, the DNA sequence used was a 17-mer (5'-GTGGAGTAGTGTCATGT-3'). Using *NUPACK* with input parameters of 24° C, 50 mM NaCl and 5 mM $MgCl_2$ (matching the salt concentrations in the PuB buffer used for incubation), a Gibbs free energy of ΔG = -24.56 kcal/mol was determined. Based on this value and the findings of Taylor et al., it can be assumed that the half-life of this connection is at least greater than 7 hours and likely extends into the range of several days, particularly when stored at lower temperatures.

Another potential explanation for the observed results is the degradation of DNA caused by freezing and thawing events. Chung et al. [68] investigated whether

freezing and freeze/thaw cycles affected DNA integrity. Using optical tweezers to simulate mechanical interactions between DNA and biomolecules, they measured the mean lifetimes of their samples, which correspond to the average time required for a double-stranded DNA (dsDNA) to break. They found that after one freeze/thaw cycle the mean lifetime of their samples at a tension of 5 pN reduced from 133.2 min (no freezing) to 44.3 min. At 15 pN tension the mean lifetimes reduced from 78.5 min (no freezing) to 10.8 min. Another study [69] investiagted the impact of repeated freeze/thaw cycles on short oligonucleotide strands, demonstrating that repeated freezing and thawing caused degradation of the samples.

To determine whether freezing and thawing of DNA origami platforms is responsible for the reduced pMHC binding efficiency observed with the two-day functionalization protocol, a future experiment is recommended. This experiment should compare functionalized platforms stored at 4°C with those stored at -20°C to assess the effect of storage conditions on platform integrity and binding efficiency.

5.4. SLB Functionalization

Despite the fact that functionalization of SLBs with modified cholesterol-DNA strands is the preferred method for anchoring DNA origami platforms, as it allows for precise control over platform orientation through specific anchor points, the measured surface densities exhibited significant fluctuations using this technique. To address this issue, a $MgCl_2$ mediated functionalization approach, taken from Hu et al. [63], was explored, with the aim of increasing cholesterol binding stability.

The idea behind combining these two approaches was, that $MgCl_2$ could reinforce cholesterol binding, resulting in a more robust anchoring and reducing the likelihood of detachment. Additionally, $MgCl_2$ could act as a secondary binding mechanism in cases where cholesterol alone might be insufficient. The experimental results demonstrated, that this approach led to improved surface densities and showed greater consistency in routine utilization, minimizing fluctuations in platform attachment.

An important question that remains is the extent to which the addition of $MgCl_2$ increases nonspecific platform binding. While the increase in surface density can be attributed to more stable anchoring, it is also possible that a fraction of DNA origami platforms may bind in an incorrect orientation solely through $MgCl_2$ interactions. Regardless, mediating cholesterol anchoring through the addition of $MgCl_2$, appears to be a promising method for enhancing SLB functionalization.

Another key modification in the adapted protocol was the timing of BSA blocking, as well as the amount of BSA used for this process. In the original method,

SLBs were passivated with BSA only after incubation with modified cholesterol strands. In the adjusted approach, SLBs were first passivated with BSA, before the addition of cholesterol strands. This adaption aimed to prevent cholesterol strands from interacting with defects in the bilayer and potentially getting trapped in them. By passivating the surface beforehand, the functionalization process was expected to be more efficient and controlled. The amount of BSA used was reduced from 1 % to 0.1 %. The original value of 1 % BSA was taken from [1], however, it was speculated that such high amounts could possibly affect membrane quality. As neither diffusion values nor surface density were negatively affected by the reduction of BSA, the change was incorporated into the protocol as well as routine work.

6. Conclusion & Outlook

T-cell activation remains a topic of ongoing investigation in the scientific community. The model system in this project was designed to explore whether preclustering of pMHC ligands facilitates T-cell activation. To address this question, essential steps in creating and optimizing a reliable model system were investigated. The system utilizes DNA origami platforms and SLBs to mimic a biological environment and precisely control the spatial arrangements of the ligands. Establishing a robust protocol for these processes is fundamental, as it provides a foundation for future research into the mechanisms of T-cell activation.

The main areas of focus in this project included the thermal folding process of DNA origami, the purification of folded platforms, the functionalization of DNA origami platforms, and the anchoring of platforms to SLBs. Each of these steps was carefully analyzed and optimized to improve reliability and reproducibility. An optimized thermal folding protocol was developed, with a focus on reliability as well as time efficiency. Ultra-filtration was identified as a more efficient purification method than agarose gel electrophoresis due to its reduced labor intensity and time requirements. Platform anchoring was found to be more stable when mediating cholesterol anchoring with $MgCl_2$, and platform binding efficiency of pMHC was found to be clearly higher when functionalizing platforms on the day of the experiment. This work provided valuable insights into the mechanics of each process and offered evidence-based recommendations on the most suitable methods depending on the specific use case.

Despite its potential, DNA origami remains a challenging tool to implement in laboratory settings due to its complex, multi-step production process. This makes it even more important to develop clear and reliable protocols to ensure consistent results. The findings of this thesis contribute to this goal by addressing several key steps in the DNA origami workflow and improving the reproducibility of the model system.

Future experiments should investigate the impact of strand age on DNA origami yield and the influence of storage temperature on platform integrity and binding efficiency. These studies could further improve our understanding of these factors affecting DNA origami stability and functionality.

In summary, this work represents an important step toward developing a reliable protocol for creating a DNA origami-based model system to study T-cell activation. The next phase will involve implementing the recommended steps and testing this

protocol with T-cells to broaden our understanding of how spatial organization influences immune signaling.

Bibliography

[1] Joschka Hellmeier. 'DNA origami as a nanoscale tool for T-cell activation'. PhD thesis. Technical University of Vienna, 2020.

[2] C. Janeway and P. Travers. *Immunobiology: The Immune System in Health and Disease*. Current Biology Limited, 1994. ISBN: 9780815316916. URL: https://books.google.at/books?id=fTJnQgAACAAJ.

[3] Juan-Manuel Anaya et al. *Autoimmunity. From Bench to Bedside*. July 2013. ISBN: 978-958-738-376-8.

[4] Himanshu Kumar, Taro Kawai and Shizuo Akira. 'Pathogen Recognition by the Innate Immune System'. In: *International Reviews of Immunology* 30 (1 Jan. 2011), pp. 16–34. ISSN: 08830185. DOI: 10.3109/08830185.2010.529976. URL: https://www.tandfonline.com/doi/abs/10.3109/08830185.2010.529976.

[5] B. Alberts et al. *Molecular Biology of the Cell 4th Edition: International Student Edition*. Routledge, 2002. ISBN: 9780815332886. URL: https://books.google.at/books?id=ozigkQEACAAJ.

[6] Veysel Kayser and Iqbal Ramzan. 'Vaccines and vaccination: history and emerging issues'. In: *Human Vaccines Immunotherapeutics* 17 (12 2021), p. 5255. ISSN: 2164554X. DOI: 10.1080/21645515.2021.1977057. URL: https://pmc.ncbi.nlm.nih.gov/articles/PMC8903967/.

[7] Abdul Abbas and Lichtman Andrew. *Basic immunology : functions and disorders of the immune system*. July 2009. ISBN: 9781416046882.

[8] Estelle Bettelli et al. 'Reciprocal developmental pathways for the generation of pathogenic effector TH17 and regulatory T cells'. In: *Nature* 441 (7090 Apr. 2006), pp. 235–238. ISSN: 1476-4687. DOI: 10.1038/nature04753. URL: https://www.nature.com/articles/nature04753.

[9] Lawrence J. Stern and Don C. Wiley. 'Antigenic peptide binding by class I and class II histocompatibility proteins'. In: *Structure* 2 (4 1994), pp. 245–251. ISSN: 0969-2126. DOI: 10.1016/S0969-2126(00)00026-5. URL: https://pubmed.ncbi.nlm.nih.gov/8087551/.

[10] Simon J. Davis and P. Anton van der Merwe. 'The kinetic-segregation model: TCR triggering and beyond'. In: *Nature Immunology* 7 (8 July 2006), pp. 803–809. ISSN: 1529-2916. DOI: 10.1038/ni1369. URL: https://www.nature.com/articles/ni1369.

[11] Dibyendu Kumar Das et al. 'Force-dependent transition in the T-cell receptor β-subunit allosterically regulates peptide discrimination and pMHC bond lifetime'. In: *Proceedings of the National Academy of Sciences of the United States of America* 112 (5 Feb. 2015), pp. 1517–1522. ISSN: 10916490. DOI: https://doi.org/10.1073/pnas.1424829112. URL: https://www.pnas.org/doi/abs/10.1073/pnas.1424829112.

[12] Timothy W. Mckeithan. 'Kinetic proofreading in T-cell receptor signal transduction.' In: *Proceedings of the National Academy of Sciences* 92 (11 May 1995), pp. 5042–5046. ISSN: 00278424. DOI: 10.1073/PNAS.92.11.5042. URL: https://www.pnas.org/doi/abs/10.1073/pnas.92.11.5042.

[13] Salvatore Valitutti et al. 'Serial triggering of many T-cell receptors by a few peptide–MHC complexes'. In: *Nature* 375 (6527 May 1995), pp. 148–151. ISSN: 1476-4687. DOI: 10.1038/375148a0. URL: https://www.nature.com/articles/375148a0.

[14] David R. Fooksman. 'Organizing MHC class II presentation'. In: *Frontiers in Immunology* 5 (APR Apr. 2014), p. 85712. ISSN: 16643224. DOI: 10.3389/FIMMU.2014.00158/BIBTEX. URL: www.frontiersin.org.

[15] Jesse Goyette et al. 'How does T cell receptor clustering impact on signal transduction?' In: *Journal of Cell Science* 132 (4 Feb. 2019). ISSN: 14779137. DOI: 10.1242/JCS.226423/57563.

[16] Gabriele Campi, Rajat Varma and Michael L. Dustin. 'Actin and agonist MHC-peptide complex-dependent T cell receptor microclusters as scaffolds for signaling'. In: *The Journal of Experimental Medicine* 202 (8 Oct. 2005), pp. 1031–1036. ISSN: 0022-1007. DOI: 10.1084/JEM.20051182. URL: https://pubmed.ncbi.nlm.nih.gov/16216891/.

[17] Tadashi Yokosuka et al. 'Newly generated T cell receptor microclusters initiate and sustain T cell activation by recruitment of Zap70 and SLP-76'. In: *Nature Immunology* 6 (12 Dec. 2005), pp. 1253–1262. ISSN: 1529-2908. DOI: 10.1038/NI1272. URL: https://pubmed.ncbi.nlm.nih.gov/16273097/.

[18] Mario Brameshuber et al. 'Monomeric TCRs drive T cell antigen recognition'. In: *Nature Immunology* 19 (5 Apr. 2018), pp. 487–496. ISSN: 1529-2916. DOI: 10.1038/s41590-018-0092-4. URL: https://www.nature.com/articles/s41590-018-0092-4.

[19] Francesca Giannoni et al. 'Clustering of T Cell Ligands on Artificial APC Membranes Influences T Cell Activation and Protein Kinase C ϑ Translocation to the T Cell Plasma Membrane'. In: *The Journal of Immunology* 174 (6 Mar. 2005), pp. 3204–3211. ISSN: 0022-1767. DOI: 10.4049/JIMMUNOL.174.6.3204. URL: https://dx.doi.org/10.4049/jimmunol.174.6.3204.

[20] Imre Gombos et al. 'Rafting MHC-II domains in the APC (presynaptic) plasma membrane and the thresholds for T-cell activation and immunological synapse formation'. In: *Immunology Letters* 92 (1-2 Mar. 2004), pp. 117–124. ISSN: 0165-2478. DOI: 10.1016/J.IMLET.2003.11.022.

[21] N.A. Campbell et al. *Biology: A Global Approach, Global Edition*. Pearson Education, 2017. ISBN: 9781292170442. URL: https://books.google.at/books?id=IJgHDgAAQBAJ.

[22] Matthew Cobb and Nathaniel Comfort. 'What Rosalind Franklin truly contributed to the discovery of DNA's structure'. In: *Nature* 616 (7958 Apr. 2023), pp. 657–660. ISSN: 14764687. DOI: 10.1038/d41586-023-01313-5. URL: https://www.nature.com/articles/d41586-023-01313-5.

[23] G.M. Cooper. *The Cell: A Molecular Approach*. The Cell: A Molecular Approach. ASM Press, 2000. ISBN: 9780878931064. URL: https://books.google.at/books?id=DCdyQgAACAAJ.

[24] J.D. Watson and T.A. Baker. *Molecular Biology of the Gene*. Pearson Education, 2008. ISBN: 9780321507815. URL: https://books.google.at/books?id=mpjZkQEACAAJ.

[25] S. Tom Pricaux. *nanotechnology*. Oct. 2024. URL: https://www.britannica.com/technology/nanotechnology.

[26] Nadrian C. Seeman and Hanadi F. Sleiman. 'DNA nanotechnology'. In: *Nature Reviews Materials* 3 (1 Nov. 2017), pp. 1–23. ISSN: 2058-8437. DOI: 10.1038/natrevmats.2017.68. URL: https://www.nature.com/articles/natrevmats201768.

[27] Nadrian C. Seeman. 'Nucleic acid junctions and lattices'. In: *Journal of Theoretical Biology* 99 (2 Nov. 1982), pp. 237–247. ISSN: 0022-5193. DOI: 10.1016/0022-5193(82)90002-9.

[28] Paul W.K. Rothemund. 'Folding DNA to create nanoscale shapes and patterns'. In: *Nature* 440 (7082 Mar. 2006), pp. 297–302. ISSN: 1476-4687. DOI: 10.1038/nature04586. URL: https://www.nature.com/articles/nature04586.

[29] Ebbe S Andersen et al. 'Self-assembly of a nanoscale DNA box with a controllable lid'. In: *Nature* 459 (7243 2009), pp. 73–76. ISSN: 1476-4687. DOI: 10.1038/nature07971. URL: https://doi.org/10.1038/nature07971.

[30] Masayuki Endo et al. 'DNA prism structures constructed by folding of multiple rectangular arms'. In: *Journal of the American Chemical Society* 131 (43 Nov. 2009), pp. 15570–15571. ISSN: 00027863. DOI: https://doi.org/10.1021/ja904252e. URL: https://pubs.acs.org/doi/full/10.1021/ja904252e.

[31] Yonggang Ke et al. 'Scaffolded DNA origami of a DNA tetrahedron molecular container'. In: *Nano Letters* 9 (6 June 2009), pp. 2445–2447. ISSN: 15306984. DOI: https://doi.org/10.1021/nl901165f. URL: https://pubs.acs.org/doi/full/10.1021/nl901165f.

[32] Grant A. Knappe, Eike Christian Wamhoff and Mark Bathe. 'Functionalizing DNA origami to investigate and interact with biological systems'. In: *Nature Reviews Materials* 8 (2 Feb. 2022), p. 123. ISSN: 20588437. DOI: 10.1038/S41578-022-00517-X. URL: https://pmc.ncbi.nlm.nih.gov/articles/PMC10191391/.

[33] Caiqing Yuan et al. 'Functionalized DNA Origami-Enabled Detection of Biomarkers'. In: *ChemBioChem* 25 (13 July 2024), e202400227. ISSN: 1439-7633. DOI: 10.1002/CBIC.202400227. URL: https://pubmed.ncbi.nlm.nih.gov/38700476/.

[34] Ralf P. Richter, Rémi Bérat and Alain R. Brisson. 'Formation of solid-supported lipid bilayers: An integrated view'. In: *Langmuir* 22 (8 Apr. 2006), pp. 3497–3505. ISSN: 07437463. DOI: https://doi.org/10.1021/la052687c. URL: https://pubs.acs.org/doi/full/10.1021/la052687c.

[35] Kabir H. Biswas and Jay T. Groves. 'Hybrid Live Cell-Supported Membrane Interfaces for Signaling Studies'. In: *Annual Review of Biophysics* 48 (Volume 48, 2019 May 2019), pp. 537–562. ISSN: 19361238. DOI: https://doi.org/10.1146/annurev-biophys-070317-033330. URL: https://www.annualreviews.org/content/journals/10.1146/annurev-biophys-070317-033330.

[36] Joshua A. Jackman and Nam Joon Cho. 'Supported Lipid Bilayer Formation: Beyond Vesicle Fusion'. In: *Langmuir* 36 (6 Feb. 2020), pp. 1387–1400. ISSN: 15205827. DOI: 10.1021/ACS.LANGMUIR.9B03706. URL: https://dx.doi.org/10.1021/acs.langmuir.9b03706.

[37] L. K. Tamm and H. M. McConnell. 'Supported phospholipid bilayers'. In: *Biophysical Journal* 47 (1 1985), pp. 105–113. ISSN: 00063495. DOI: 10.1016/S0006-3495(85)83882-0.

[38] Chiho Hamai et al. 'Effect of Average Phospholipid Curvature on Supported Bilayer Formation on Glass by Vesicle Fusion'. In: *Biophysical Journal* 90 (4 Feb. 2006), pp. 1241–1248. ISSN: 0006-3495. DOI: 10.1529/BIOPHYSJ.105.069435.

[39] Edward T. Castellana and Paul S. Cremer. 'Solid supported lipid bilayers: From biophysical studies to sensor design'. In: *Surface Science Reports* 61 (10 Nov. 2006), pp. 429–444. ISSN: 0167-5729. DOI: 10.1016/J.SURFREP.2006.06.001. URL: https://pubmed.ncbi.nlm.nih.gov/32287559/.

[40] Michael Edidin. 'Rotational and Lateral Diffusion of Membrane Proteins and Lipids: Phenomena and Function'. In: *Current Topics in Membranes and Transport* 29 (C Jan. 1987), pp. 91–127. ISSN: 0070-2161. DOI: 10.1016/S0070-2161(08)60044-1.

[41] Beata Sweryda-Krawiec et al. 'A New Interpretation of Serum Albumin Surface Passivation'. In: *Langmuir* 20 (6 Mar. 2004), pp. 2054–2056. ISSN: 07437463. DOI: https://doi.org/10.1021/la034870g. URL: https://pubs.acs.org/doi/full/10.1021/la034870g.

[42] Corden Pharma. *POPC - 1-Palmitoyl-2-Oleoyl-sn-Glycero-3-Phosphocholine*. Accessed: 2024-12-26. 2024. URL: https://cordenpharma.com/lipid-catalog/phospholipids/popc/.

[43] Shawn M. Douglas et al. 'Rapid prototyping of 3D DNA-origami shapes with caDNAno'. In: *Nucleic Acids Research* 37 (15 2009), pp. 5001–5006. ISSN: 1362-4962. DOI: 10.1093/NAR/GKP436. URL: https://pubmed.ncbi.nlm.nih.gov/19531737/.

[44] Marcus J. Taylor et al. 'A DNA-Based T Cell Receptor Reveals a Role for Receptor Clustering in Ligand Discrimination'. In: *Cell* 169 (1 Mar. 2017), 108–119.e20. ISSN: 0092-8674. DOI: 10.1016/J.CELL.2017.03.006.

[45] Carlos Ernesto Castro et al. 'A primer to scaffolded DNA origami'. In: *Nature Methods* 8 (3 Feb. 2011), pp. 221–229. ISSN: 1548-7105. DOI: 10.1038/nmeth.1570. URL: https://www.nature.com/articles/nmeth.1570.

[46] Michael J. Neuhoff et al. 'Recycling Materials for Sustainable DNA Origami Manufacturing'. In: *Nano Letters* 24 (39 Oct. 2024), pp. 12080–12087. ISSN: 1530-6984. DOI: 10.1021/ACS.NANOLETT.4C02695. URL: https://pubs.acs.org/doi/full/10.1021/acs.nanolett.4c02695.

[47] Jürgen J. Schmied et al. 'DNA origami–based standards for quantitative fluorescence microscopy'. In: *Nature Protocols* 9 (6 May 2014), pp. 1367–1391. ISSN: 1750-2799. DOI: 10.1038/nprot.2014.079. URL: https://www.nature.com/articles/nprot.2014.079.

[48] Alan Shaw, Erik Benson and Björn Högberg. 'Purification of functionalized DNA origami nanostructures'. In: *American Chemical Society Nano* 9 (5 May 2015), pp. 4968–4975. ISSN: 1936086X. DOI: 10.1021/NN507035G. URL: www.acsnano.org4968.

[49] Gaetan Bellot et al. 'Recovery of intact DNA nanostructures following agarose-gel–based separation'. In: *Nature Methods* 8 (3 Mar. 2011), 10.1038/nmeth0311–192. ISSN: 15487091. DOI: 10.1038/NMETH0311-192. URL: https://pmc.ncbi.nlm.nih.gov/articles/PMC3843644/.

[50] Chenxiang Lin et al. 'Purification of DNA-origami nanostructures by rate-zonal centrifugation'. In: *Nucleic Acids Research* 41 (2 Jan. 2012), e40. ISSN: 03051048. DOI: 10.1093/NAR/GKS1070. URL: https://pmc.ncbi.nlm.nih.gov/articles/PMC3553994/.

[51] Joschka Hellmeier et al. 'DNA origami demonstrate the unique stimulatory power of single pMHCs as T cell antigens'. In: *Proceedings of the National Academy of Sciences of the United States of America* 118 (4 2021). DOI: 10.1073/pnas.2016857118/-/DCSupplemental. URL: https://doi.org/10.1073/pnas.2016857118.

[52] R. Merkel et al. 'Energy landscapes of receptor-ligand bonds explored with dynamic force spectroscopy'. In: *Nature* 397 (6714 Jan. 1999), pp. 50–53. ISSN: 0028-0836. DOI: 10.1038/16219. URL: https://pubmed.ncbi.nlm.nih.gov/9892352/.

[53] Ernst-Ludwig Florin, Vincent T. Moy and Hermann E. Gaub. 'Adhesion Forces Between Individual Ligand-Receptor Pairs'. In: *Science* 264 (5157 Apr. 1994), pp. 415–417. ISSN: 0036-8075. DOI: 10.1126/SCIENCE.8153628. URL: https://www.science.org/doi/10.1126/science.8153628.

[54] Mark Howarth et al. 'A monovalent streptavidin with a single femtomolar biotin binding site'. In: *Nature Methods* 3 (4 Apr. 2006), p. 267. ISSN: 15487091. DOI: 10.1038/NMETHXXX. URL: https://pmc.ncbi.nlm.nih.gov/articles/PMC2576293/.

[55] Joschka Hellmeier et al. 'Strategies for the Site-Specific Decoration of DNA Origami Nanostructures with Functionally Intact Proteins'. In: *ACS Nano* 15 (9 Sept. 2021), pp. 15057–15068. ISSN: 1936086X. DOI: 10.1021/ACSNANO.1C05411/ASSET/IMAGES/MEDIUM/NN1C05411_M020.GIF. URL: https://pubs.acs.org/doi/full/10.1021/acsnano.1c05411.

[56] Julian Valero, ed. *Attachment of DNA Origami to Zwitterionic Lipid Membranes*. May 2023. Chap. 14, p. 3028. DOI: 10.1007/978-1-0716-3028-0_14. URL: https://link.springer.com/protocol/10.1007/978-1-0716-3028-0_14.

[57] Diana Morzy et al. 'Cations Regulate Membrane Attachment and Functionality of DNA Nanostructures'. In: *Journal of the American Chemical Society* 143 (19 May 2021), pp. 7358–7367. ISSN: 15205126. DOI: 10.1021/JACS.1C00166/SUPPL_FILE/JA1C00166_SI_006.AVI. URL: https://pubs.acs.org/doi/full/10.1021/jacs.1c00166.

[58] Yuki Suzuki et al. 'Dynamic assembly/disassembly processes of photoresponsive DNA origami nanostructures directly visualized on a lipid membrane surface'. In: *Journal of the American Chemical Society* 136 (5 Feb. 2014), pp. 1714–1717. ISSN: 00027863. DOI: 10.1021/JA4109819/SUPPL_FILE/JA4109819_SI_003.AVI. URL: https://pubs.acs.org/doi/full/10.1021/ja4109819.

[59] Jasleen Kaur Daljit Singh et al. 'Binding of DNA origami to lipids: maximizing yield and switching via strand displacement'. In: *Nucleic Acids Research* 49 (19 Nov. 2021), pp. 10835–10850. ISSN: 0305-1048. DOI: 10.1093/NAR/GKAB888. URL: https://dx.doi.org/10.1093/nar/gkab888.

[60] Siu Ho Wong et al. 'Modulating the DNA/Lipid Interface through Multivalent Hydrophobicity'. In: *Nano Letters* (Sept. 2024). ISSN: 15306992. DOI: 10.1021/ACS.NANOLETT.4C02564/ASSET/IMAGES/LARGE/NL4C02564_0004.JPEG. URL: https://pubs.acs.org/doi/full/10.1021/acs.nanolett.4c02564.

[61] Ammasi Periasamy. *Methods in Cellular Imaging*. Oxford University Press, 2001.

[62] Stephen T. Ross et al. *Total Internal Reflection Fluorescence (TIRF) Microscopy*. Nov. 2024.

[63] Yuesong Hu et al. 'Quantifying T cell receptor mechanics at membrane junctions using DNA origami tension sensors'. In: *Nature Nanotechnology* 19 (11 Aug. 2024), pp. 1674–1685. ISSN: 1748-3395. DOI: 10.1038/s41565-024-01723-0. URL: https://www.nature.com/articles/s41565-024-01723-0.

[64] Guido Van Rossum and Fred L Drake Jr. *Python reference manual*. Centrum voor Wiskunde en Informatica Amsterdam, 1995.

[65] Lukas Schrangl. *sdt-python: Python library for fluorescence microscopy data analysis*. Version 15.2. https://doi.org/10.5281/zenodo.4604495. Oct. 2020. DOI: 10.5281/zenodo.4604495.

[66] Elena Georgiou et al. 'DNA Origami – Lipid Membrane Interactions Controlled by Nanoscale Sterics'. In: *Small* 20 (42 Oct. 2024), p. 2404720. ISSN: 1613-6829. DOI: 10.1002/SMLL.202404720. URL: https://onlinelibrary.wiley.com/doi/full/10.1002/smll.202404720.

[67] Joseph N. Zadeh et al. 'NUPACK: Analysis and design of nucleic acid systems'. In: *Journal of Computational Chemistry* 32 (1 Jan. 2011), pp. 170–173. ISSN: 1096-987X. DOI: https://doi.org/10.1002/jcc.21596. URL: https://onlinelibrary.wiley.com/doi/full/10.1002/jcc.21596%20https://onlinelibrary.wiley.com/doi/abs/10.1002/jcc.21596%20https://onlinelibrary.wiley.com/doi/10.1002/jcc.21596.

[68] Wei Ju Chung et al. 'Freezing shortens the lifetime of DNA molecules under tension'. In: *Journal of Biological Physics* 43 (4 Dec. 2017), p. 511. ISSN: 15730689. DOI: 10.1007/S10867-017-9466-3. URL: https://pmc.ncbi.nlm.nih.gov/articles/PMC5696304/.

[69] D. L. Davis, E. P. O'Brien and C. M. Bentzley. 'Analysis of the degradation of oligonucleotide strands during the freezing/thawing processes using MALDI-MS'. In: *Analytical chemistry* 72 (20 Oct. 2000), pp. 5092–5096. ISSN: 0003-2700. DOI: 10.1021/AC000225S. URL: https://pubmed.ncbi.nlm.nih.gov/11055733/.

List of Abbreviations

AF488 Alexa Fluor^{TM} 488

AF555 Alexa Fluor^{TM} 555

AF647 Alexa Fluor^{TM} 647

APC antigen-presenting cell

AS635P abberior STAR 635P

BSA bovine serum albumin

CAD computer-aided design

CTC cytotoxic T-cell

DAMP damage-associated molecular pattern

DGS-NTA(Ni) 1,2-dioleoyl-sn-glycero-3-[(N-(5-amino-1-carboxypentyl)iminodiacetic acid)succinyl](nickle salt)

DNA deoxyribonucleic acid

dsDNA double stranded DNA

DOPE 1,2-dioleoyl-sn-glycero-3-phosphoethanolamine

DPBD dulbecco's phosphate buffered saline

FoB folding buffer

His polyhistidine

HSC haematopoietic stem cell

ICAM intercellular adhesion molecule

LTC Nunc^{TM} Lab-Tek chamber

MHC major histocompatibility complex

$MgCl_2$ magnesium chloride

mSA monovalent streptavidin

MSD mean squared displacement

PAMP pathogen-associated molecular pattern

PCR polymerase chain reaction

pMHC peptide-major histocompatibility complex

POPC 1-palmitoyl-2-oleoyl-glycero-3-phosphocholine

PRR pathogen recognition pattern

PuB purification buffer

ROI region of interest

sem standard error of the mean

SLB supported lipid bilayer

SMB single molecule brightness

ssDNA single stranded DNA

SUV small unilamellar vesicle

TCR T-cell receptor

TIR total internal reflection

TIRF total internal reflection fluorescence

List of Figures

List of Tables

A. Supplementary Information

Table A.1.: **DNA origami mixing table 1**

Components	DNA strands	Amount [µL]	Final concentration
Scaffold	-	10	10 nM
FoB	-	10	$1x$
$MgCl_2$	-	1.25	12.5 mM
Mastemix	134	26.8	100 nM/strand
Yellow no corners	35	6	100 nM/strand
X' mix	6	1.2	100 nM/strand
Z' mix	8	1.6	100 nM/strand
Yellow 25	1	0.2	100 nM/strand
Yellow S	5	1	100 nM/strand
X-fluorophor	6	3	250 nM/strand
UP H_2O	-	39	
Total volume	-	100	

Table A.2.: **DNA origami mixing table 2**

Components	DNA strands	Amount [µl]	Final concentration
Scaffold	-	10	10 nM
FoB	-	10	$1x$
$MgCl_2$	-	1.25	12.5 mM
Mastemix	134	26.8	100 nM/strand
Yellow topmix	36	7.2	100 nM/strand
Z' mix	8	1.6	100 nM/strand
Yellow 25	1	0.2	100 nM/strand
Yellow S	5	1	100 nM/strand
UP H_2O	-	41.9	
Total volume	-	100	

Table A.3.: **DNA origami mixing table 3**

Components	DNA strands	Amount [µL]	Final concentration
Scaffold	-	10	10 nM
FoB	-	10	$1x$
$MgCl_2$	-	1.25	12.5 mM
Mastemix	134	13.4	100 nM/strand
Yellow no corners	35	3.5	100 nM/strand
X' mix	6	0.6	100 nM/strand
Z' mix	8	0.8	100 nM/strand
V' mix	1	0.1	100 nM/strand
Yellow S	5	0.5	100 nM/strand
X-fluorophor	6	1.5	250 nM/strand
UP H_2O	-	58.85	
Total volume	-	100	

Table A.4.: **DNA origami mixing table 4**

Components	DNA strands	Amount [µL]	Final concentration
Scaffold	-	30	30 nM
FoB	-	10	$1x$
$MgCl_2$	-	1	10 mM
Mastemix	134	40.2	300 nM/strand
Yellow no corners	35	10.5	300 nM/strand
X' mix	6	1.8	300 nM/strand
Z' mix	8	2.4	300 nM/strand
V' mix	1	0.3	300 nM/strand
Yellow S	5	1.5	300 nM/strand
X-fluorophor	6	3.6	600 nM/strand
V-fluorophore	1	0.6	600 nM/strand
Total volume	-	100	

Table A.5.: **List of staple strands.**

DNA Oligno Name	DNA Sequence
MASTER MIX	
21[32]23[31]	TTTTCACTCAAAGGGCGAAAAACCATCACC
3[32]5[31]	AATACGTTTGAAAGAGGACAGACTGACCTT
1[32]3[31]	AGGCTCCAGAGGCTTTGAGGACACGGGTAA
0[47]1[31]	AGAAAGGAACAACTAAAGGAATTCAAAAAAA
19[32]21[31]	GTCGACTTCGGCCAACGCGCGGGGTTTTTC
17[32]19[31]	TGCATCTTTCCCAGTCACGACGGCCTGCAG
15[32]17[31]	TAATCAGCGGATTGACCGTAATCGTAACCG
13[32]15[31]	AACGCAAAATCGATGAACGGTACCGGTTGA
11[32]13[31]	AACAGTTTTGTACCAAAAACATTTTATTTC
9[32]11[31]	TTTACCCCAACATGTTTTAAATTTCCATAT
7[32]9[31]	TTTAGGACAAATGCTTTAAACAATCAGGTC
5[32]7[31]	CATCAAGTAAAACGAACTAACGAGTTGAGA
6[47]4[48]	TACGTTAAAGTAATCTTGACAAGAACCGAACT
2[47]0[48]	ACGGCTACAAAAGGAGCCTTTAATGTGAGAAT
22[47]20[48]	CTCCAACGCAGTGAGACGGGCAACCAGCTGCA
18[47]16[48]	CCAGGGTTGCCAGTTTGAGGGGACCCGTGGGA
14[47]12[48]	AACAAGAGGGATAAAAATTTTTAGCATAAAGC
10[47]8[48]	CTGTAGCTTGACTATTATAGTCAGTTCATTGA
21[56]23[63]	AGCTGATTGCCCTTCAGAGTCCACTATTAAAGGGTGCCGT
1[64]4[64]	TTTATCAGGACAGCATCGGAACGACACCAACCTAAAACGAGGTCAATC
0[79]1[63]	ACAACTTTCAACAGTTTCAGCGGATGTATCGG
15[64]18[64]	GTATAAGCCAACCCGTCGGATTCTGACGACAGTATCGGCCGCAAGGCG
13[64]15[63]	TATATTTTGTCATTGCCTGAGAGTGGAAGATT
11[64]13[63]	GATTTAGTCAATAAAGCCTCAGAGAACCCTCA
9[64]11[63]	CGGATTGCAGAGCTTAATTGCTGAAACGAGTA
7[56]9[63]	ATGCAGATACATAACGGGAATCGTCATAAATAAAGCAAAG
6[79]4[80]	TTATACCACCAAATCAACGTAACGAACGAG
2[79]0[80]	CAGCGAAACTTGCTTTCGAGGTGTTGCTAA
22[79]20[80]	TGGAACAACCGCCTGGCCCTGAGGCCCGCT
18[79]16[80]	GATGTGCTTCAGGAAGATCGCACAATGTGA
14[79]12[80]	GCTATCAGAAATGCAATGCCTGAATTAGCA
10[79]8[80]	GATGGCTTATCAAAAAGATTAAGAGCGTCC
21[96]23[95]	AGCAAGCGTAGGGTTGAGTGTTGTAGGGAGCC
3[96]5[95]	ACACTCATCCATGTTACTTAGCCGAAAGCTGC
1[96]3[95]	AAACAGCTTTTTGCGGGATCGTCAACACTAAA
0[111]1[95]	TAAATGAATTTTCTGTATGGGATTAATTTCTT
19[96]21[95]	CTGTGTGATTGCGTTGCGCTCACTAGAGTTGC
17[96]19[95]	GCTTTCCGATTACGCCAGCTGGCGGCTGTTTC
15[96]17[95]	ATATTTTGGCTTTCATCAACATTATCCAGCCA
13[96]15[95]	TAGGTAAACTATTTTTGAGAGATCAAACGTTA
11[96]13[95]	AATGGTCAACAGGCAAGGCAAAGAGTAATGTG
9[96]11[95]	CGAAAGACTTTGATAAGAGGTCATATTTCGCA
7[96]9[95]	TAAGAGCAAATGTTTAGACTGGATAGGAAGCC
5[96]7[95]	TCATTCAGATGCGATTTTAAGAACAGGCATAG
6[111]4[112]	ATTACCTTTGAATAAGGCTTGCCCAAATCCGC
2[111]0[112]	AAGGCCGCTGATACCGATAGTTGCGACGTTAG
22[111]20[112]	GCCCGAGAGTCCACGCTGGTTTGCAGCTAACT
18[111]16[112]	TCTTCGCTGCACCGCTTCTGGTGCGGCCTTCC
14[111]12[112]	GAGGGTAGGATTCAAAAGGGTGAGACATCCAA
10[111]8[112]	TTGCTCCTTTCAAATATCGCGTTTGAGGGGGT

DNA Oligno Name	DNA Sequence
21[120]23[127]	CCCAGCAGGCGAAAAATCCCTTATAAATCAAGCCGGCG
1[128]4[128]	TGACAACTCGCTGAGGCTTGCATTATACCAAGCGCGATGATAAA
0[143]1[127]	TCTAAAGTTTTGTCGTCTTTCCAGCCGACAA
15[128]18[128]	TAAATCAAAATAATTCGCGTCTCGGAAACCAGGCAAAGGGAAGG
13[128]15[127]	GAGACAGCTAGCTGATAAATTAATTTTTGT
11[128]13[127]	TTTGGGGATAGTAGTAGCATTAAAAGGCCG
9[128]11[127]	GCTTCAATCAGGATTAGAGAGTTATTTTCA
7[120]9[127]	CGTTTACCAGACGACAAAGAAGTTTTGCCATAATTCGA
3[160]4[144]	TTGACAGGCCACCACCAGAGCCGCGATTTGTA
0[175]0[144]	TCCACAGACAGCCCTCATAGTTAGCGTAACGA
19[160]20[144]	GCAATTCACATATTCCTGATTATCAAAGTGTA
15[160]16[144]	ATCGCAAGTATGTAAATGCTGATGATAGGAAC
11[160]12[144]	CCAATAGCTCATCGTAGGAATCATGGCATCAA
7[160]8[144]	TTATTACGAAGAACTGGCATGATTGCGAGAGG
23[128]23[159]	AACGTGGCGAGAAAGGAAGGGAAACCAGTAA
6[143]5[159]	GATGGTTTGAACGAGTAGTAAATTTACCATTA
4[143]3[159]	TCATCGCCAACAAAGTACAACGGACGCCAGCA
2[143]1[159]	ATATTCGGAACCATCGCCCACGCAGAGAAGGA
22[143]21[159]	TCGGCAAATCCTGTTTGATGGTGGACCCTCAA
20[143]19[159]	AAGCCTGGTACGAGCCGGAAGCATAGATGATG
18[143]17[159]	CAACTGTTGCGCCATTCGCCATTCAAACATCA
16[143]15[159]	GCCATCAAGCTCATTTTTTAACCACAAATCCA
14[143]13[159]	CAACCGTTTCAAATCACCATCAATTCGAGCCA
12[143]11[159]	TTCTACTACGCGAGCTGAAAAGGTTACCGCGC
10[143]9[159]	CCAACAGGAGCGAACCAGACCGGAGCCTTTAC
8[143]7[159]	CTTTTGCAGATAAAAACCAAAATAAAGACTCC
6[175]4[176]	CAGCAAAAGGAAACGTCACCAATGAGCCGC
2[175]0[176]	TATTAAGAAGCGGGGTTTTGCTCGTAGCAT
22[175]20[176]	ACCTTGCTTGGTCAGTTGGCAAAGAGCGGA
18[175]16[176]	CTGAGCAAAAATTAATTACATTTTGGGTTA
14[175]12[176]	CATGTAATAGAATATAAAGTACCAAGCCGT
10[175]8[176]	TTAACGTCTAACATAAAAACAGGTAACGGA
21[184]23[191]	TCAACAGTTGAAAGGAGCAAATGAAAAATCTAGAGATAGA
1[192]4[192]	GCGGATAACCTATTATTCTGAAACAGACGATTGGCCTTGAAGAGCCAC
0[207]1[191]	TCACCAGTACAAACTACAACGCCTAGTACCAG
15[192]18[192]	TCAAATATAACCTCCGGCTTAGGTAACAATTTCATTTGAAGGCGAATT
13[192]15[191]	GTAAAGTAATCGCCATATTTAACAAAACTTTT
11[192]13[191]	TATCCGGTCTCATCGAGAACAAGCGACAAAAG
9[192]11[191]	TTAGACGGCCAAATAAGAAACGATAGAAGGCT
7[184]9[191]	CGTAGAAAATACATACCGAGGAAACGCAATAAGAAGCGCA
6[207]4[208]	TCACCGACGCACCGTAATCAGTAGCAGAACCG
2[207]0[208]	TTTCGGAAGTGCCGTCGAGAGGGTGAGTTTCG
22[207]20[208]	AGCCAGCAATTGAGGAAGGTTATCATCATTTT
18[207]16[208]	CGCGCAGATTACCTTTTTTAATGGGAGAGACT
14[207]12[208]	AATTGAGAATTCTGTCCAGACGACTAAACCAA
10[207]8[208]	ATCCCAATGAGAATTAACTGAACAGTTACCAG
21[224]23[223]	CTTTAGGGCCTGCAACAGTGCCAATACGTG
3[224]5[223]	TTAAAGCCAGAGCCGCCACCCTCGACAGAA
1[224]3[223]	GTATAGCAAACAGTTAATGCCCAATCCTCA
0[239]1[223]	AGGAACCCATGTACCGTAACACTTGATATAA
19[224]21[223]	CTACCATAGTTTGAGTAACATTTAAAATAT
17[224]19[223]	CATAAATCTTTGAATACCAAGTGTTAGAAC
15[224]17[223]	CCTAAATCAAAATCATAGGTCTAAACAGTA
13[224]15[223]	ACAACATGCCAACGCTCAACAGTCTTCTGA

DNA Oligno Name	DNA Sequence
11[224]13[223]	GCGAACCTCCAAGAACGGGTATGACAATAA
9[224]11[223]	AAAGTCACAAAATAAACAGCCAGCGTTTTA
7[224]9[223]	AACGCAAAGATAGCCGAACAAACCCTGAAC
5[224]7[223]	TCAAGTTTCATTAAAGGTGAATATAAAAGA
6[239]4[240]	GAAATTATTGCCTTTAGCGTCAGACCGGAACC
2[239]0[240]	GCCCGTATCCGGAATAGGTGTATCAGCCCAAT
22[239]20[240]	TTAACACCAGCACTAACAACTAATCGTTATTA
18[239]16[240]	CCTGATTGCAATATATGTGAGTGATCAATAGT
14[239]12[240]	AGTATAAAGTTCAGCTAATGCAGATGTCTTTC
10[239]8[240]	GCCAGTTAGAGGGTAATTGAGCGCTTTAAGAA
21[248]23[255]	AGATTAGAGCCGTCAAAAAACAGAGGTGAGGCCTATTAGT
1[256]4[256]	CAGGAGGTGGGGTCAGTGCCTTGAGTCTCTGAATTTACCGGGAACCAG
0[271]1[255]	CCACCCTCATTTTCAGGGATAGCAACCGTACT
15[256]18[256]	GTGATAAAAAGACGCTGAGAAGAGATAACCTTGCTTCTGTTCGGGAGA
13[256]15[255]	GTTTATCAATATGCGTTATACAAACCGACCGT
11[256]13[255]	GCCTTAAACCAATCAATAATCGGCACGCGCCT
9[256]11[255]	GAGAGATAGAGCGTCTTTCCAGAGGTTTTGAA
7[248]9[255]	GTTTATTTTGTCACAATCTTACCGAAGCCCTTTAATATCA
23[256]22[272]	CTTTAATGCGCGAACTGATAGCCCCACCAG
6[271]4[272]	ACCGATTGTCGGCATTTTCGGTCATAATCA
4[271]2[272]	AAATCACCTTCCAGTAAGCGTCAGTAATAA
2[271]0[272]	GTTTTAACTTAGTACCGCCACCCAGAGCCA
22[271]20[272]	CAGAAGATTAGATAATACATTTGTCGACAA
20[271]18[272]	CTCGTATTAGAAATTGCGTAGATACAGTAC
18[271]16[272]	CTTTTACAAAATCGTCGCTATTAGCGATAG
16[271]14[272]	CTTAGATTTAAGGCGTTAAATAAAGCCTGT
14[271]12[272]	TTAGTATCACAATAGATAAGTCCACGAGCA
12[271]10[272]	TGTAGAAATCAAGATTAGTTGCTCTTACCA
10[271]8[272]	ACGCTAACACCCACAAGAATTGAAAATAGC
8[271]6[272]	AATAGCTATCAATAGAAAATTCAACATTCA
YELLOW NO CORNERS	
23[32]22[48]	CAAATCAAGTTTTTTGGGGTCGAAACGTGGA
4[47]2[48]	GACCAACTAATGCCACTACGAAGGGGGTAGCA
20[47]18[48]	TTAATGAACTAGAGGATCCCCGGGGGGTAACG
12[47]10[48]	TAAATCGGGATTCCCAATTCTGCGATATAATG
23[64]22[80]	AAAGCACTAAATCGGAACCCTAATCCAGTT
20[79]18[80]	TTCCAGTCGTAATCATGGTCATAAAAGGGG
16[79]14[80]	GCGAGTAAAAATATTTAAATTGTTACAAAG
12[79]10[80]	AAATTAAGTTGACCATTAGATACTTTTGCG
8[79]6[80]	AATACTGCCCAAAAGGAATTACGTGGCTCA
23[96]22[112]	CCCGATTTAGAGCTTGACGGGGAAAAAGAATA
4[111]2[112]	GACCTGCTCTTTGACCCCCAGCGAGGGAGTTA
20[111]18[112]	CACATTAAAATTGTTATCCGCTCATGCGGGCC
16[111]14[112]	TGTAGCCATTAAAATTCGCATTAAATGCCGGA
8[111]6[112]	AATAGTAAACACTATCATAACCCTCATTGTGA
21[160]22[144]	TCAATATCGAACCTCAAATATCAATTCCGAAA
1[160]2[144]	TTAGGATTGGCTGAGACTCCTCAATAACCGAT
23[160]22[176]	TAAAAGGGACATTCTGGCCAACAAAGCATC
4[175]2[176]	CACCAGAAAGGTTGAGGCAGGTCATGAAAG
20[175]18[176]	ATTATCATTCAATATAATCCTGACAATTAC
16[175]14[176]	TATAACTAACAAAGAACGCGAGAACGCCAA
8[175]6[176]	ATACCCAACAGTATGTTAGCAAATTAGAGC
23[192]22[208]	ACCCTTCTGACCTGAAAGCGTAAGACGCTGAG
20[207]18[208]	GCGGAACATCTGAATAATGGAAGGTACAAAAT
16[207]14[208]	ACCTTTTTATTTTAGTTAATTTCATAGGGCTT
12[207]10[208]	GTACCGCAATTCTAAGAACGCGAGTATTATTT
8[207]6[208]	AAGGAAACATAAAGGTGGCAACATTATCACCG

DNA Oligno Name	DNA Sequence
23[224]22[240]	GCACAGACAATATTTTTGAATGGGGTCAGTA
4[239]2[240]	GCCTCCCTCAGAATGGAAAGCGCAGTAACAGT
16[239]14[240]	GAATTTATTTAATGGTTTGAAATATTCTTACC
12[239]10[240]	CTTATCATTCCCGACTTGCGGGAGCCTAATTT
YELLOW TOPMIX	
23[32]22[48]	CAAATCAAGTTTTTTGGGGTCGAAACGTGGA
4[47]2[48]	GACCAACTAATGCCACTACGAAGGGGGTAGCA
20[47]18[48]	TTAATGAACTAGAGGATCCCCGGGGGGGTAACG
16[47]14[48]	ACAAACGGAAAAGCCCCAAAAACACTGGAGCA
12[47]10[48]	TAAATCGGGATTCCCAATTCTGCGATATAATG
8[47]6[48]	ATCCCCCTATACCACATTCAACTAGAAAAATC
23[64]22[80]	AAAGCACTAAATCGGAACCCTAATCCAGTT
4[79]2[80]	GCGCAGACAAGAGGCAAAAGAATCCCTCAG
20[79]18[80]	TTCCAGTCGTAATCATGGTCATAAAAGGGG
16[79]14[80]	GCGAGTAAAAATATTTAAATTGTTACAAAG
12[79]10[80]	AAATTAAGTTGACCATTAGATACTTTTGCG
8[79]6[80]	AATACTGCCCAAAAGGAATTACGTGGCTCA
23[96]22[112]	CCCGATTTAGAGCTTGACGGGGAAAAAGAATA
4[111]2[112]	GACCTGCTCTTTGACCCCCAGCGAGGGAGTTA
20[111]18[112]	CACATTAAAATTGTTATCCGCTCATGCGGGCC
16[111]14[112]	TGTAGCCATTAAAATTCGCATTAAATGCCGGA
8[111]6[112]	AATAGTAAACACTATCATAACCCTCATTGTGA
21[160]22[144]	TCAATATCGAACCTCAAATATCAATTCCGAAA
1[160]2[144]	TTAGGATTGGCTGAGACTCCTCAATAACCGAT
23[160]22[176]	TAAAAGGGACATTCTGGCCAACAAAGCATC
4[175]2[176]	CACCAGAAAGGTTGAGGCAGGTCATGAAAG
20[175]18[176]	ATTATCATTCAATATAATCCTGACAATTAC
16[175]14[176]	TATAACTAACAAAGAACGCGAGAACGCCAA
8[175]6[176]	ATACCCAACAGTATGTTAGCAAATTAGAGC
23[192]22[208]	ACCCTTCTGACCTGAAAGCGTAAGACGCTGAG
4[207]2[208]	CCACCCTCTATTCACAAACAAATACCTGCCTA
20[207]18[208]	GCGGAACATCTGAATAATGGAAGGTACAAAAT
16[207]14[208]	ACCTTTTTATTTTAGTTAATTTCATAGGGCTT
12[207]10[208]	GTACCGCAATTCTAAGAACGCGAGTATTATTT
8[207]6[208]	AAGGAAACATAAAGGTGGCAACATTATCACCG
23[224]22[240]	GCACAGACAATATTTTTGAATGGGGTCAGTA
4[239]2[240]	GCCTCCCTCAGAATGGAAAGCGCAGTAACAGT
20[239]18[240]	ATTTTAAAATCAAAATTATTTGCACGGATTCG
16[239]14[240]	GAATTTATTTAATGGTTTGAAATATTCTTACC
12[239]10[240]	CTTATCATTCCCGACTTGCGGGAGCCTAATTT
8[239]6[240]	AAGTAAGCAGACACCACGGAATAATATTGACG

DNA Oligno Name	DNA Sequence
YELLOW S	
12|11|10|112]	TAAATCATATAACCTGTTTAGCTAACCTTTAA
17|16|18|144]	AGAAAACAAAGAAGATGATGAAACAGGCTGCG
9|160|0|144]	AGAGAGAAAAAAATGAAAATAGCAAGCAAACT
5|160|6|144]	GCAAGGCCTCACCAGTAGCACCATGGGCTTGA
YELLOW 25	
13|160|14|144]	GTAATAAGTTAGGCAGAGGCATTTATGATATT
X' MIX	
12|47|0|48|-4T-X'	GCGCAGACAAGAGGCAAAAGAATCCCTCAGTTTTGCCAAGATAGACAGAAG
4|47|2|48|-4T-X'	ACAAACGGAAAAGCCCCAAAAAACACTGGAGCATTTTGCCAAGATAGACAGAAG
20|79|18|80|-4T-X'	ATCCCCCTATACCACATTCAACTAGAAAAATCTTTTGCCAAGATAGACAGAAG
12|175|10|176|-4T-X'	CCACCCTCTATTCACAAACAAATACCTGCCTATTTTGCCAAGATAGACAGAAG
20|239|18|240|-4T-X'	ATTTTTAAAATCAAAATTATTTGCACGGATTCGTTTTGCCAAGATAGACAGAAG
8|239|6|240|-4T-X'	AAGTAAGCAGACACCACGGAATAATATTGACGTTTTGCCAAGATAGACAGAAG
Z' MIX	
18|63|20|56|-4T-Z'	ATTAAGTTTACCGAGCTCGAATTCGGGAAACCTGTCGTGCTTTTAGAGTCCTAGCATATTTAGCC
4|63|6|56|-4T-Z'	ATAAGGGAACCGGATATTCATTACGTCAGGACGTTGGGAATTTTAGAGTCCTAGCATATTTAGCC
18|127|20|120|-4T-Z'	GCGATCGGCAATTCCACACAACAGGTGCCTAATGAGTGTTTTAGAGTCCTAGCATATTTAGCC
4|127|6|120|-4T-Z'	TTGTGTCGTCACGAGAAACACCAAATTTCAACTTTAATTTTTAGAGTCCTAGCATATTTAGCC
18|191|20|184|-4T-Z'	ATTCATTTTTGTTTGGATTATACTAAGAAACCACCAGAAGTTTTTAGAGTCCTAGCATATTTAGCC
4|191|6|184|-4T-Z'	CACCCTCAGAAACCATCGATAGCATTGAGCCATTTGGGAATTTTTAGAGTCCTAGCATATTTAGCC
18|255|20|248|-4T-Z'	AACAATAACGTAAAACAGAAATAAAAATCCTTTGCCCGAATTTTTAGAGTCCTAGCATATTTAGCC
4|255|6|248|-4T-Z'	AGCCACCACTGTAGCGCGTTTTTCAAGGGAGGGAAGGTAAATTTTTAGAGTCCTAGCATATTTAGCC
V' MIX	
13|160|14|144|-4T-V'	GTAATAAGTTAGGCAGAGGCATTTATGATATTTTTTGTGAGTAGTGTCATGT

B. Use of AI

Table B.1.: **Use of generative AI.** The following table provides an overview of the use of generative AI in this work. AI was used as an assisting tool in this work, with the focus on finding papers discussing certain topics, as well as rephrasing paragraphs in order to improve the reading flow.

Language model	**Version**	**Prompt**	**Use in Work**
ChatGPT	ChatGPT-4o	Rewrite the following praragraph in a clear and cohrerent manner	Chapter 1 Chapter 2.1 Chapter 2.2.3 Chapter 2.3 Chapter 3.1.3.1 Chapter 4.3
ChatGPT	ChatGPT-4o	Find papers discussing the following topic	Platform anchoring via $MgCl_2$ T-cell maturation Thermal folding of Origami Ultra-filtration